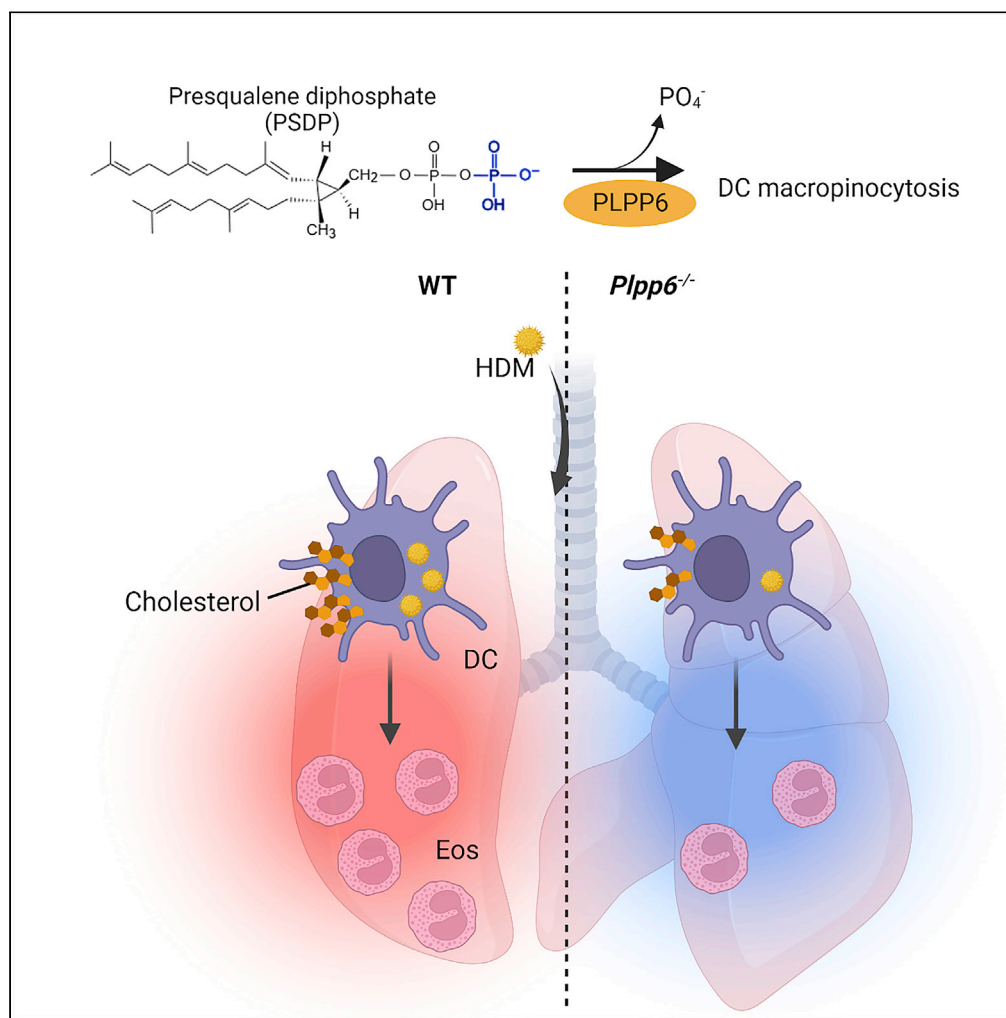


Article

Mouse phospholipid phosphatase 6 regulates dendritic cell cholesterol, macropinocytosis, and allergen sensitization



Thayse R. Brüggenmann, Troy Carlo, Nandini Krishnamoorthy, ..., Byoungsook Goh, Sungwhan F. Oh, Bruce D. Levy

blevy@bwh.harvard.edu

Highlights

Mouse *Plpp6* converts presqualene diphosphate into presqualene monophosphate

Mouse *Plpp6* is regulated during allergic lung inflammation

Plpp6^{-/-} DCs have lower cholesterol content and decreased allergen macropinocytosis

Plpp6^{-/-} mice have decreased allergic lung inflammation in response to HDM

Brüggenmann et al., iScience
25, 105185
October 21, 2022 © 2022
<https://doi.org/10.1016/j.isci.2022.105185>

Article

Mouse phospholipid phosphatase 6 regulates dendritic cell cholesterol, macropinocytosis, and allergen sensitization

Thayse R. Brüggemann,¹ Troy Carlo,¹ Nandini Krishnamoorthy,¹ Melody G. Duvall,¹ Raja-Elie E. Abdounour,¹ Julie Nijmeh,¹ Hong Yong Peh,¹ Harilaos Filippakis,¹ Roxanne H. Croze,¹ Byoungsook Goh,² Sungwhan F. Oh,² and Bruce D. Levy^{1,3,*}

SUMMARY

Lipid phosphate phosphatases are a family of enzymes with diverse cellular metabolic functions. Phospholipid phosphatase 6 (PLPP6) is a regulator of cellular polyisoprenyl phosphates; however, its *in vivo* functions remain to be determined. Here, mouse PLPP6 was characterized to possess similar catalytic properties as the human enzyme. *Plpp6* knockout mice (*Plpp6*^{-/-}) were generated and displayed decreased airway allergen sensitization, pointing to a role for PLPP6 in the early events of lung allergic responses. Dendritic cell (DC) responses were investigated and endocytosis of allergen via macropinocytosis was decreased in *Plpp6*^{-/-} DCs that had lower cholesterol content. When reversed by cholesterol loading, the DC macropinocytosis defect is corrected. Adoptive transfer of *Plpp6*^{-/-} DCs to wild-type mice during sensitization was sufficient to decrease allergen-induced responses. Together, our findings have identified PLPP6 as a pivotal regulator of DC cholesterol content and macropinocytosis, cellular mechanisms that are important for pathologic responses in allergen-induced lung inflammation.

INTRODUCTION

Phospholipid phosphatase 6 (PLPP6) is an enzyme that is regulated in human inflammation (Gordon et al., 2016; <https://asthma.cellgeni.sanger.ac.uk/>, Access date: December 10 2021) with its role *in vivo* to be established. PLPP6 was originally characterized in human neutrophils (Fukunaga et al., 2006; Levy et al., 1997) and is also expressed in lung dendritic cells (DCs) (Heng et al., 2008), suggesting functional roles for PLPP6 in these immune cells. Lung DCs patrol the airway, which is a mucosal barrier that is regularly exposed to inhaled challenges. Inhaled particles become immersed in airway lining liquid and are constitutively internalized by lung DCs via macropinocytosis as part of their sentinel function (Sallusto et al., 1995). Lung DCs can initiate immune responses, which if inappropriate or excessive can cause immunopathology (Nathan, 2002), such as the allergic responses underlying asthma (Fahy, 2015; Fanta, 2009). The lipid composition of cell membranes is important for normal cell function (Maxfield and Tabas, 2005). Cholesterol is an important determinant of membrane organization (Maxfield and Tabas, 2005) and epithelial cell macropinocytosis (Grimmer et al., 2002). DCs loaded with cholesterol efficiently internalize and present antigens to prime naive lymphocytes (Fessler, 2015; Packard et al., 2008). Thus, regulatory mechanisms for cholesterol content of lung DCs have the potential to limit DC antigen uptake via macropinocytosis and restrain adaptive allergic responses.

Cellular cholesterol content can be regulated by several biochemical feedback mechanisms (Brown and Goldstein, 1980). Select polyisoprenyl diphosphates (PIPPs) are cholesterol biosynthetic intermediates with feedback regulatory properties (Levy et al., 1997, 1999). In addition to cholesterol metabolism, PIPPs serve vital cellular functions, including as intracellular signals for inflammatory responses (Levy et al., 1997). One member of this class of PIPP metabolites is presqualene diphosphate (PSDP) that upon cell activation is rapidly and transiently converted to presqualene monophosphate (PSMP) by PLPP6 (Fukunaga et al., 2006; Levy et al., 1997). PSMP is 2–3 log orders less potent than PSDP in inhibiting phospholipase D and phosphoinositol-3 kinase, important signaling molecules in cell activation (Bonnans

¹Pulmonary and Critical Care Medicine, Department of Internal Medicine, Brigham and Women's Hospital and Harvard Medical School, Boston, MA 02115, USA

²Center for Experimental Therapeutics and Reperfusion Injury, Department of Internal Medicine, Brigham and Women's Hospital and Harvard Medical School, Boston, MA 02115, USA

³Lead contact

*Correspondence:

blevy@bwh.harvard.edu

<https://doi.org/10.1016/j.isci.2022.105185>



et al., 2006; Levy et al., 1999). Thus, targeting PLPP6 may regulate PIPP metabolism, cholesterol biosynthesis, and cell function.

Here, we have identified and characterized a murine homolog of human PLPP6, including its expression and catalytic actions on PIPPs and related phosphorylated lipids. By generating a mouse strain deficient in *Plpp6*, we have uncovered a pivotal role for murine *Plpp6* as a regulator of cell cholesterol, DC macrophinocytosis, and allergen-induced lung inflammation.

RESULTS

Plpp6 gene expression and activity are regulated during inflammation

When human cells are activated, PSDP is rapidly converted by PLPP6 to PSMP (Fukunaga et al., 2006; Levy et al., 1997) (Figure 1A). To investigate *in vivo* roles for PLPP6, the mouse homolog of human PLPP6 was identified and determined to be 87.5% identical at the amino acid level, including 100% homology for the critical catalytic domains (C1, C2, and C3) (Figure S1A). To determine if the putative mouse *Plpp6* shared the enzymatic activity and substrate preference of human PLPP6 (Fukunaga et al., 2006), recombinant mouse *Plpp6* was overexpressed in HEK293 cells. Upon exposure to a range of phosphorylated lipids, including PSDP, sphingosine-1-phosphate (S1P), farnesyl diphosphate (FDP), phosphatidic acid (PA), and lysophosphatidic acid (LPA), mouse *Plpp6* gave a similar rank order for substrate preference as human PLPP6 (Figure 1B) (Carlo et al., 2009; Fukunaga et al., 2006). In the presence of PSDP, *Plpp6* released 5.05 ± 2.65 nmol/mg/min phosphate with significantly lower activity for structurally related substrates with a rank order of PSDP >>> PA > S1P > FDP > LPA (Figure 1B).

To determine if *Plpp6* gene expression was regulated *in vivo* during tissue inflammation, allergic lung inflammation was induced in wild-type (WT) mice by sensitization and challenge with house dust mite extract (HDM) (Figure 1C). 24h after the last HDM challenge (protocol day 16), lung *Plpp6* expression was markedly lower than in baseline antigen naive lungs (Figure 1D). Of note, lung gene expression of related PLPP family members *Plpp1*, *Plpp2*, *Plpp3*, *Plpp4* and *Plpp5* were also decreased during the inflammatory response (Figure S1B). To selectively investigate roles for *Plpp6* in inflammation, *Plpp6* deficient mice (*Plpp6*^{-/-}) were generated by the replacement of the mouse *Plpp6* coding sequence with a neomycin cassette (see STAR Methods, Figures S1C and S1D). Homozygous *Plpp6*^{-/-} mice were viable and *Plpp6* heterozygous and homozygous deficient mice litters segregated as expected (Figure S1E). *Plpp6*^{-/-} and WT mice had no significant differences in the expression of the other related PLPP family members (Figure S1F). After HDM sensitization and challenge, lung tissue was harvested, and non-saponifiable lipids were assessed by thin-layer chromatography (TLC) (see STAR Methods). In WT mice, lung PSMP levels were higher than PSDP levels after HDM sensitization and challenge (Figures S1G and S1H). In contrast, the same HDM protocol for allergic lung inflammation in *Plpp6*^{-/-} mice led to lung PSMP levels that were lower than PSDP levels (Figures S1G and S1H). Of interest, the amounts of lung PSMP by TLC densitometry were similar between WT and *Plpp6*^{-/-} mice (Figures S1G and S1H). To confirm the densitometric measures of PSMP in lung tissue, samples were analyzed by LC-MS/MS (Figure 1E). After HDM sensitization and challenge, LC-MS/MS revealed that lung PSMP levels increased approximately 2-fold in WT mice compared to antigen-naïve baseline levels, whereas PSMP levels in *Plpp6*^{-/-} mice after HDM sensitization and challenge were still similar to the WT baseline levels (Figure 1F). These changes in polyisoprenyl phosphates (PIPPs) did not reach statistical significance at these small sample sizes but were consistent with the results from isolated recombinant m*Plpp6* (Figure 1B) and suggested decreased conversion of PSDP to PSMP with *Plpp6* deficiency. Together, these data indicate that m*Plpp6* is a PIPP phosphatase and that *Plpp6* expression and activity are regulated during allergic lung inflammation.

Plpp6^{-/-} mice have decreased serum and cell cholesterol

Given that PSDP is an essential biosynthetic intermediate for cholesterol (Figure 2A), we next investigated if the changes in PIPP remodeling in the *Plpp6*^{-/-} mice impacted cholesterol levels. Serum total cholesterol (free cholesterol and cholesteryl esters) levels were measured in *Plpp6*^{-/-} and WT mice receiving standard chow (see STAR Methods) at baseline and on day 16 of the HDM protocol. *Plpp6*^{-/-} mice had lower serum total cholesterol levels compared to WT mice at baseline and the levels remained low in the *Plpp6*^{-/-} mice after HDM sensitization and challenge (Figure 2B). Serum total cholesterol levels in WT mice decreased significantly with peak allergic inflammation (HDM day 16), approximately to levels found in the *Plpp6*^{-/-} mice (Figure 2B), likely as a consequence of the decreased *Plpp6* expression after HDM (Figure 1D). No significant differences were apparent at baseline between *Plpp6*^{-/-} and WT mice in lung expression of

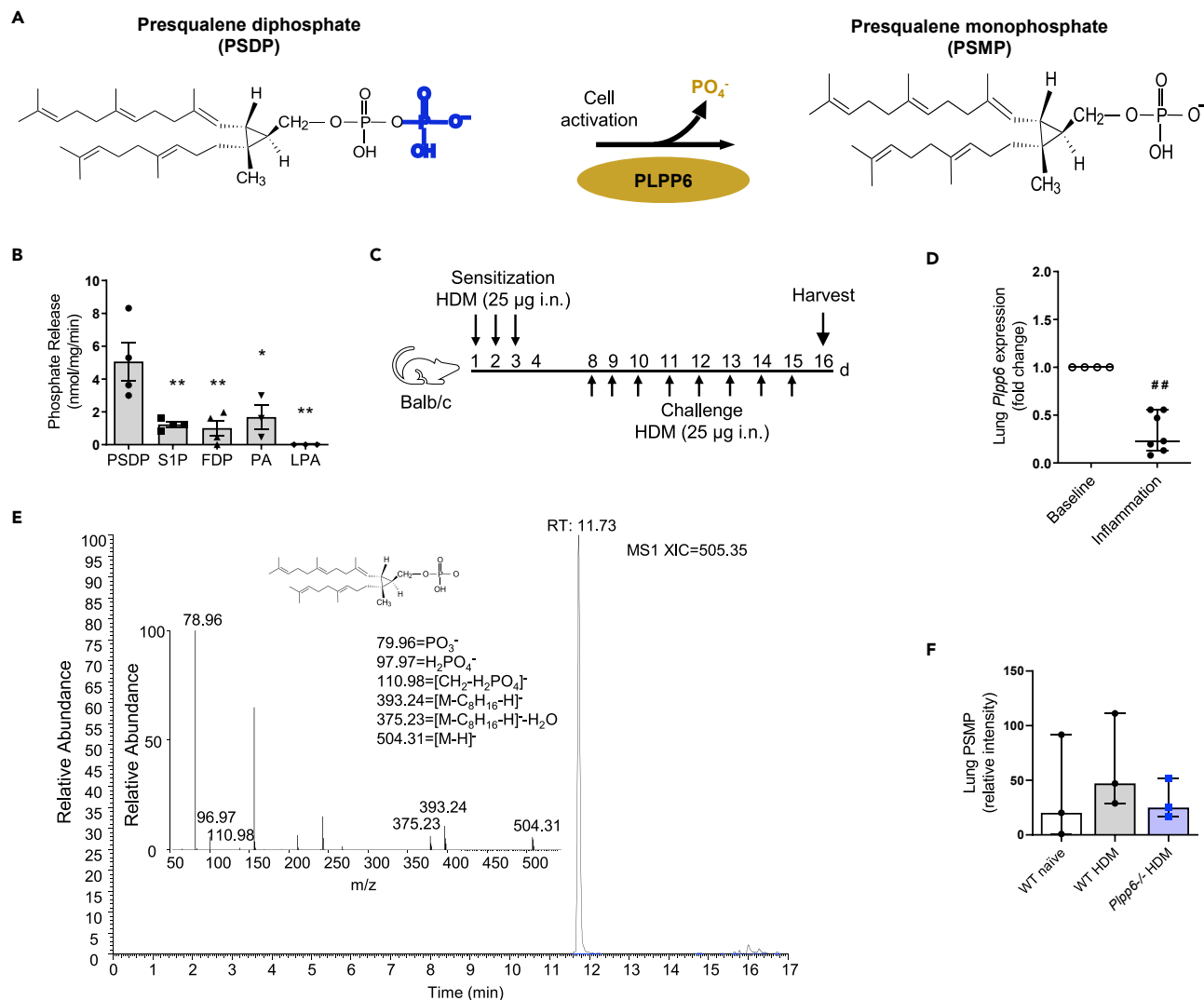


Figure 1. Murine *Plpp6* gene expression and activity is regulated during inflammation

(A) PLPP6 converts presqualene diphosphate (PSDP) into presqualene monophosphate (PSMP) upon cell activation.

(B) Phosphate release from PSDP, sphingosine-1-phosphate (S1P), farnesyl diphosphate (FDP), phosphatidic acid (PA), and lysophosphatidic acid (LPA) exposed to recombinant murine PLPP6 (see STAR Methods); experiments were performed 4 times for a total of $n = 3$ to 4.

(C) Allergic lung inflammation model with house dust mite (HDM) exposure (see STAR Methods).

(D) Lung *Plpp6* expression in WT mice on day 16 of HDM protocol; experiments were performed 2 times for a total of $n = 4$ to 7; data represent fold change relative to baseline expression.

(E) Extracted ion chromatogram (MS-XIC) and MS/MS assignment of isolated PSMP ($[\text{M-H}] = 505.35$).

(F) PSMP content in lungs from WT and *Plpp6*^{-/-} mice on day 16 of HDM protocol; results are expressed as fold change to the mean value of PSMP in the naive group of the same genotype; experiments were performed 3 times for a total of $n = 3$. * $p < 0.05$ and ** $p < 0.01$ comparing S1P, FDP, PA, LPA to PSDP by one-way ANOVA and Tukey test for multiple comparisons. ## $p < 0.01$ comparing inflammation to baseline by unpaired nonparametric Mann-Whitney test. Bars represent median with interquartile range. See also Figure S1.

several biosynthetic and metabolic enzymes for PIPPs and cholesterol (Figure S2A). Of interest, at protocol day 16 of the HDM allergic lung inflammation model, lung expression of these cholesterol biosynthetic enzymes in *Plpp6*^{-/-} mice was significantly decreased to a greater extent than in WT mice (Figure S2B). Together, these findings indicate that *Plpp6* expression can regulate cholesterol biosynthetic enzymes and cholesterol serum levels.

Given the relationship between PLPP6 and cholesterol biosynthetic enzyme expression, we next looked at cellular cholesterol levels and flux. Because lung DCs are limited in number, we assessed DC cholesterol

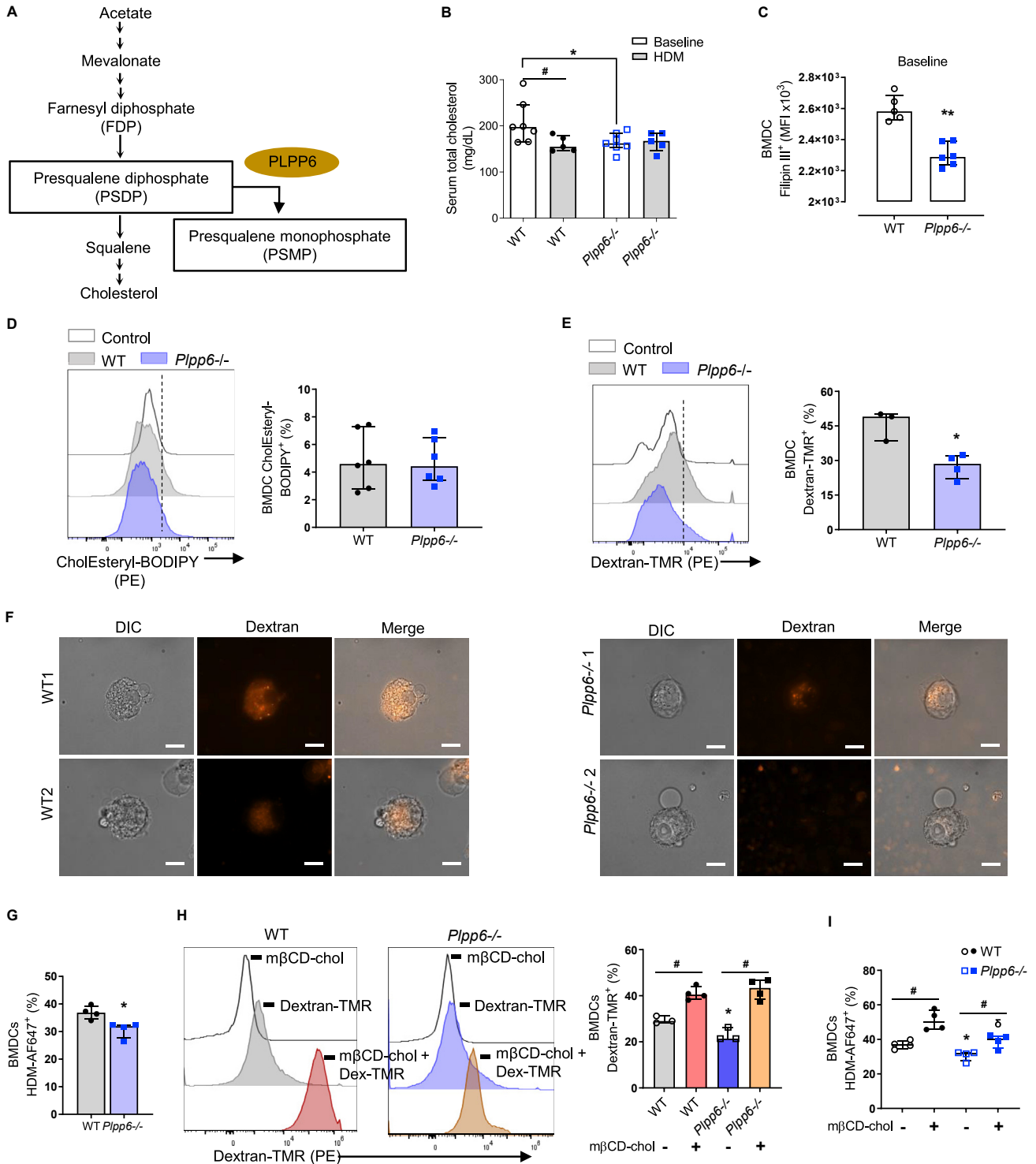


Figure 2. *Plpp6*^{-/-} mice have decreased serum, DC cholesterol, and macropinocytosis

(A) Cholesterol biosynthesis pathway; PLPP6 converts PSDP, a biosynthetic intermediate for cholesterol, into PSMP upon cell activation.

(B) Serum total cholesterol at baseline and on day 16 of HDM protocol was measured by colorimetric assay (see STAR Methods); experiments were performed 3 times for a total of n = 7.

(C) BMDC free cholesterol content was measured by Filipin III staining and analyzed by flow cytometry; experiments were performed 3 times for a total of n = 5 to 6.

Figure 2. Continued

(D) LDLR-mediated cholesterol transport was determined using BMDCs exposed to CholEsteryl-BODIPY and analyzed by flow cytometry; percentage of CholEsteryl-BODIPY⁺ BMDCs are shown (see STAR Methods) (representative flow cytometry histograms on the left); experiments were performed 3 times for a total of n = 6.

(E) BMDC macropinocytosis of dextran (70,000 MW)-TMR was analyzed by flow cytometry; percentage of dextran-TMR⁺ BMDCs (representative flow cytometry histograms on the left); experiments were performed 2 times for a total of n = 3 to 4.

(F) Representative confocal microscopy images of WT and *Plpp6*^{-/-} BMDCs exposed to dextran-TMR; images of DIC, fluorescent and merged channels; scale bars correspond to 10 μm.

(G) BMDC uptake of fluorescent-labeled HDM (HDM-AF647) analyzed by flow cytometry; percentage of HDM-AF647⁺ BMDCs; experiments were performed 2 times for a total of n = 4.

(H) WT and *Plpp6*^{-/-} BMDC cholesterol content were experimentally increased using methyl-beta-cyclodextrin loaded cholesterol (mβCD-chol) (160 μg/mL of cholesterol) (See STAR Methods) before incubation with labeled dextran; percentage of dextran-TMR⁺ BMDCs were quantitated by FACS (representative flow cytometry histograms on the left); experiments were performed 3 times for a total of n = 4.

(I) WT and *Plpp6*^{-/-} BMDC exposed to mβCD-chol (See STAR Methods) before incubation with labeled HDM; percentage of HDM-AF647⁺ BMDCs were quantitated by FACS; experiments were performed 2 times for a total of n = 4. *p < 0.05, **p < 0.05, #p = 0.05 by unpaired nonparametric Mann-Whitney test. Bars represent median with interquartile range. See also Figure S2.

levels in bone marrow-derived DCs (BMDCs) that were generated *in vitro* from WT and *Plpp6*^{-/-} mice (see STAR Methods). Using Filipin III to measure free cholesterol content (see STAR Methods), *Plpp6*^{-/-} BMDCs had significantly lower Filipin III staining relative to WT BMDCs, consistent with decreased cholesterol content (Figure 2C). Because cell size may influence cholesterol content, the size of WT and *Plpp6*^{-/-} BMDCs was determined using ImageJ and showed no difference in cell size between genotypes (Figure S2C). We next determined the ability of the *Plpp6*^{-/-} BMDCs to import exogenous cholesterol by low-density lipoprotein receptor (LDLR)-dependent transport of a fluorescent cholesterol ester analog (CholEsteryl-BODIPY). Using flow cytometry analysis, we found no significant differences between the *Plpp6*^{-/-} BMDCs relative to WT cells (Figure 2D), indicating that distinct from cholesterol biosynthesis, lack of *Plpp6* expression did not limit LDLR mediated cholesterol uptake.

***In vitro* macropinocytosis is reduced in *Plpp6*^{-/-} dendritic cells**

As cell cholesterol is an integral component of membrane lipid rafts that are essential for endocytosis (Maxfield and Tabas, 2005), we next determined the effect of *Plpp6* expression on DC function. *Plpp6*^{-/-} and WT BMDC uptake of tetramethylrhodamine (TMR)-labeled dextran (70,000 MW) (dextran-TMR) was measured *in vitro* because this process proceeds selectively by macropinocytosis (Commisso et al., 2014). Dextran-TMR uptake by *Plpp6*^{-/-} BMDCs was significantly decreased by approximately 50% relative to WT BMDCs (Figures 2E, 2F, and S2D). BMDCs exposed to 5-(N-ethyl-N-isopropyl)-amiloride (EIPA), a macropinocytosis-specific inhibitor (Commisso et al., 2014), markedly inhibited dextran-TMR uptake irrespective of genotype (Figure S2E). The uptake of labeled HDM (HDM-AF647) was also lower in *Plpp6*^{-/-} BMDCs compared to WT cells (Figure 2G). EIPA inhibited BMDC HDM-AF647 uptake by both WT and *Plpp6*^{-/-} BMDCs to the point where significant genotype-specific differences were no longer evident (Figure S2F). Of note, the decrease in *Plpp6*^{-/-} BMDC macropinocytosis was not associated with visually evident changes in filopodia and lamellipodia formation or membrane ruffling, as shown in Video S1 and S2.

To determine if the lower cellular cholesterol levels in *Plpp6*^{-/-} BMDCs were related to their decreased endocytosis, the cells were loaded with exogenous cholesterol and challenged with dextran-TMR (see STAR Methods). BMDC cholesterol content was increased using methyl-β-cyclodextrin loaded cholesterol (mβCD-chol) (160 μg of cholesterol per mL) and this exogenous cholesterol loading significantly increased both WT and *Plpp6*^{-/-} BMDC macropinocytosis of dextran-TMR (Figure 2H). In addition, increasing BMDC cholesterol content also increased the uptake of HDM-AF647 by *Plpp6*^{-/-} BMDCs (Figure 2I). Together, these data indicate that decreased *Plpp6* expression can reduce cellular cholesterol content and significantly decrease DC allergen uptake.

***Plpp6*^{-/-} mice have reduced lung inflammatory responses to allergen**

To determine if the *in vitro* changes in the *Plpp6*^{-/-} DC function translated to *in vivo* changes in inflammation, WT and *Plpp6*^{-/-} mice were immunophenotyped after airway HDM sensitization and challenge. Compared to WT, *Plpp6*^{-/-} mice had decreased allergic lung inflammation 24h after the HDM challenge with decreased tissue leukocyte infiltration and mucous cell metaplasia (Figure 3A). Changes in lung leukocyte numbers and differential were assessed by flow cytometry (gating strategy in Figure S3A, see STAR Methods). Relative to antigen-naïve mice, total lung leukocytes (CD45⁺ cells) were increased on HDM protocol day 16 in WT and

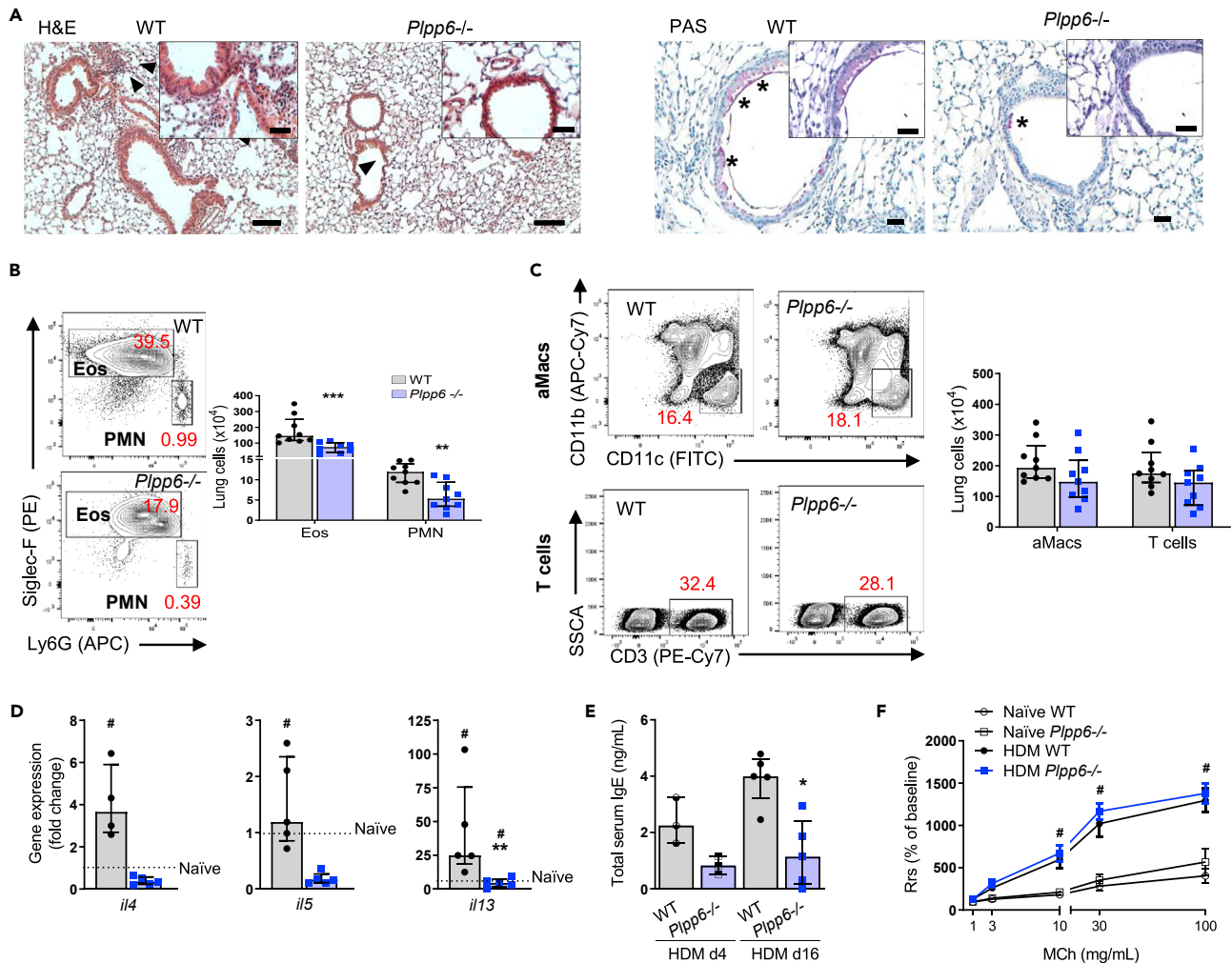


Figure 3. *Plpp6*^{-/-} mice have reduced lung inflammatory responses to allergen

(A–D) *Plpp6*^{-/-} and WT mice were airway sensitized and challenged with HDM and their immunophenotype was determined on protocol day 16—a time of increased allergic lung inflammation. (A) Representative images of lung histology after staining with hematoxylin and eosin (H&E), arrowheads indicate leukocyte infiltration (left panels), or with periodic acid schiff (PAS), asterisks indicate mucous cells metaplasia (right panels); scale bars correspond to 100 μ m in 10x images (H&E) and 20x images (PAS) and 50 μ m in 40x images. (B) Lung differential cell numbers of eosinophils (Eos) and neutrophils (PMN) were determined by FACS (representative contour plots on the left; numbers in red represent the percentage of leukocytes); experiments were performed 3 times for a total of n = 9. (C) Lung differential cell numbers of alveolar macrophages (aMacs) and T cells determined by FACS (representative contour plots on the left; numbers in red represent the percentage of leukocytes); experiments were performed 3 times for a total of n = 9 (see Figure S3A for gating strategy). (D) Gene expression of *il4*, *il5*, and *il13* by RT-qPCR in lung tissue harvested on protocol day 16; data represent fold change in gene expression with HDM relative to naive within the same genotype; experiments were performed 3 times for a total of n = 4 to 5.

(E) Total serum IgE was measured by ELISA on days 4 and 16 of the HDM protocol; experiments were performed 2 times for a total of n = 3 to 5.

(F) Resistance of the respiratory system (Rrs) was determined by invasive measurement in anesthetized animals by Flexivent in response to increasing doses of methacholine (MCh) (1, 3, 10, 30, and 100 mg/mL); experiments were performed 2 times for a total of n = 4 to 9; data represent percent change from baseline. *p < 0.05, **p < 0.01 and ***p < 0.001 comparing WT and *Plpp6*^{-/-}, and #p < 0.05 comparing HDM and naive within same mouse genotype by unpaired nonparametric Mann-Whitney test. Bars represent median with interquartile range in (B–E) and mean \pm SE in (F). See also Figure S3.

Plpp6^{-/-} mice; however, the increased leukocyte numbers were significantly lower in *Plpp6*^{-/-} mice compared to WT (Figures S3B–S3D). Lung eosinophils (Eos) and neutrophils (PMN) were significantly lower in *Plpp6*^{-/-} mice and no significant changes were present in alveolar macrophage (aMacs) or total T cell numbers relative to WT (Figures 3B and 3C). Lung mRNA expression of the type 2 cytokines *il4*, *il5*, and *il13* was significantly decreased in *Plpp6*^{-/-} mice relative to WT after the HDM challenge (Figure 3D). Lung homogenate cytokines were assessed by ELISA. There were trends for decreased levels of IL-5 and IL-13 in *Plpp6*^{-/-} mice relative to WT on protocol day 16 (Figure S3E) that were not as marked as the changes in mRNA

expression at this time point (Figure 2D). Similar trends for decreased type 2 cytokine expression were also present in lung CD4⁺ T cells and ILC2s (Figures S3F and S3G). No changes were apparent in mediastinal lymph node (MLN) CD4⁺ T cell cytokine expression (Figure S3H). Total serum IgE was significantly decreased in *Plpp6*^{-/-} mice after HDM sensitization and challenge (protocol day 16) (Figure 3E). Because IgE levels were decreased, memory B cell numbers were quantitated in lungs, MLNs, and spleen and found to be similar in *Plpp6*^{-/-} and WT mice (Figures S4A and S4B). Of interest, airway hyperresponsiveness (AHR) to methacholine (MCh) was not significantly different between *Plpp6*^{-/-} and WT mice after HDM; the mean ED₂₀₀ (the effective dose of MCh required to double pulmonary resistance) for MCh was 2.44 ± 1.93 in *Plpp6*^{-/-} and 3.14 ± 2.53 in WT (Figure 3F). Together, these results indicate that *Plpp6*^{-/-} mice have decreased allergic lung inflammation, and the diminished IgE levels suggest a defect in the early events of allergen sensitization from the sluggish function of *Plpp6*^{-/-} DCs (Figure 2).

Plpp6^{-/-} mice have decreased allergen-induced lung dendritic cell number and function

To determine if changes in allergic responses in *Plpp6*^{-/-} mice were related to changes in lung DC subtypes, we next investigated early *in vivo* events in allergen sensitization. At baseline and after a single HDM exposure (protocol day 2) the numbers of lung CD103⁺ DCs and monocyte-derived DCs (MoDCs) were not different between *Plpp6*^{-/-} mice and WT (Figures S5, S6A, and S6B). In contrast, at protocol day 4, lung CD103⁺ DCs and MoDCs did not increase to the same extent in *Plpp6*^{-/-} mice as WT (Figure 4A). In HDM sensitized mice, repeated HDM airway challenge further increased lung DC recruitment, but to a significantly lesser extent in *Plpp6*^{-/-} mice compared to WT (protocol day 16) (Figure 4B). Although lung DCs were relatively decreased in the *Plpp6*^{-/-} mice after HDM sensitization, the MLN DC numbers were not significantly different in WT and *Plpp6*^{-/-} mice protocol day 4 (Figure 4C). In contrast to the decreased lung DC numbers, *Plpp6*^{-/-} mice had significantly higher numbers of MLN CD103⁺ DCs and plasmacytoid DCs (pDCs) at protocol day 16 (Figure 4D). Because changes in lung and MLN DC numbers were in opposite directions in the *Plpp6*^{-/-} mice, the expression of the DC chemotactic receptor CCR7 was determined, yet no significant differences in CCR7 by flow cytometry were detected between WT and *Plpp6*^{-/-} DCs during early allergen exposure at protocol days 2 and 4 (Figures S6C and S6D).

DCs play key roles in the induction of CD4⁺ effector cells via costimulatory molecules and MHC-II antigen presentation to naive CD4⁺ T cells at the immune synapse (Walker and McKenzie, 2018). MHC-II expression was significantly lower in MLN CD103⁺ DCs and CD11b⁺ DCs in *Plpp6*^{-/-} relative to WT after one dose of HDM (protocol day 2) (Figure 4E) with further decreases upon repeated HDM exposure (protocol day 4) to a similar extent in *Plpp6*^{-/-} and WT mice (Figures 4E and S6E). CD103⁺ DCs and CD11b⁺ DCs from WT and *Plpp6*^{-/-} mice expressed similar amounts of the costimulatory molecules CD40 and CD86 at protocol day 16 (Figure S6E). To test their functional capacity to instruct naive CD4⁺ T cells to become CD4⁺ Th2 effectors, lung and MLN DCs from WT and *Plpp6*^{-/-} mice were flow sorted from allergen sensitized animals, primed with ovalbumin (OVA), and then co-cultured *in vitro* with either WT, *Plpp6*^{-/-} or DO11.10 (positive control) naive CD4⁺ T cells (Figure 4F, see STAR Methods). CD4⁺ T cells (WT or antigen-specific (DO11.10)) produced significantly lower percentages of IL-13⁺ CD4⁺ Th2 cells when co-cultured with antigen (OVA)-primed *Plpp6*^{-/-} DCs compared to WT DCs (Figures 4G and 4H). Results obtained with naive *Plpp6*^{-/-} CD4⁺ T cells gave similar trends for decrease with *Plpp6*^{-/-} relative to WT DCs (Figure 4I), suggesting that PLPP6 expression primarily impacted DC rather than T cell function in response to allergen. No significant differences in T cell proliferation were observed between the WT and *Plpp6*^{-/-} mice (Figure S6F). Together, these data indicate a functionally significant role for PLPP6 in the DC initiation of type 2 adaptive immune responses.

Plpp6^{-/-} mice have decreased *in vivo* dendritic cell allergen uptake and allergic lung inflammation

To determine if the decreased responses to HDM allergen in *Plpp6*^{-/-} DCs *in vitro* were also present *in vivo*, fluorescently labeled HDM allergen (HDM-AF647) was instilled intranasally (i.n.) and 24h later lung DC uptake was analyzed by flow cytometry (Plantinga et al., 2013) (see STAR Methods, Figure 5A). After one exposure to HDM-AF647, there were significantly lower percentages and lower numbers of HDM-AF647⁺ DCs present in the lungs of *Plpp6*^{-/-} mice (Figures 5A, 5B, and S6G). With repeated HDM exposure, differences in the number and percentage of HDM-AF647⁺ lung DCs in *Plpp6*^{-/-} mice were no longer apparent on protocol day 4 (Figures 5C, 5D, and S6H); however, at this time point, the lung DC HDM-AF647⁺ MFI was significantly decreased in *Plpp6*^{-/-} mice, particularly in CD103⁺ DCs and CD11b⁺ DCs (Figure 5E). These changes were not related to a defect in DC migration because the numbers of HDM-AF647⁺ DCs in the lung draining MLN on days 2 and 4 were not significantly decreased (Figures 5F and 5G). Similar to the

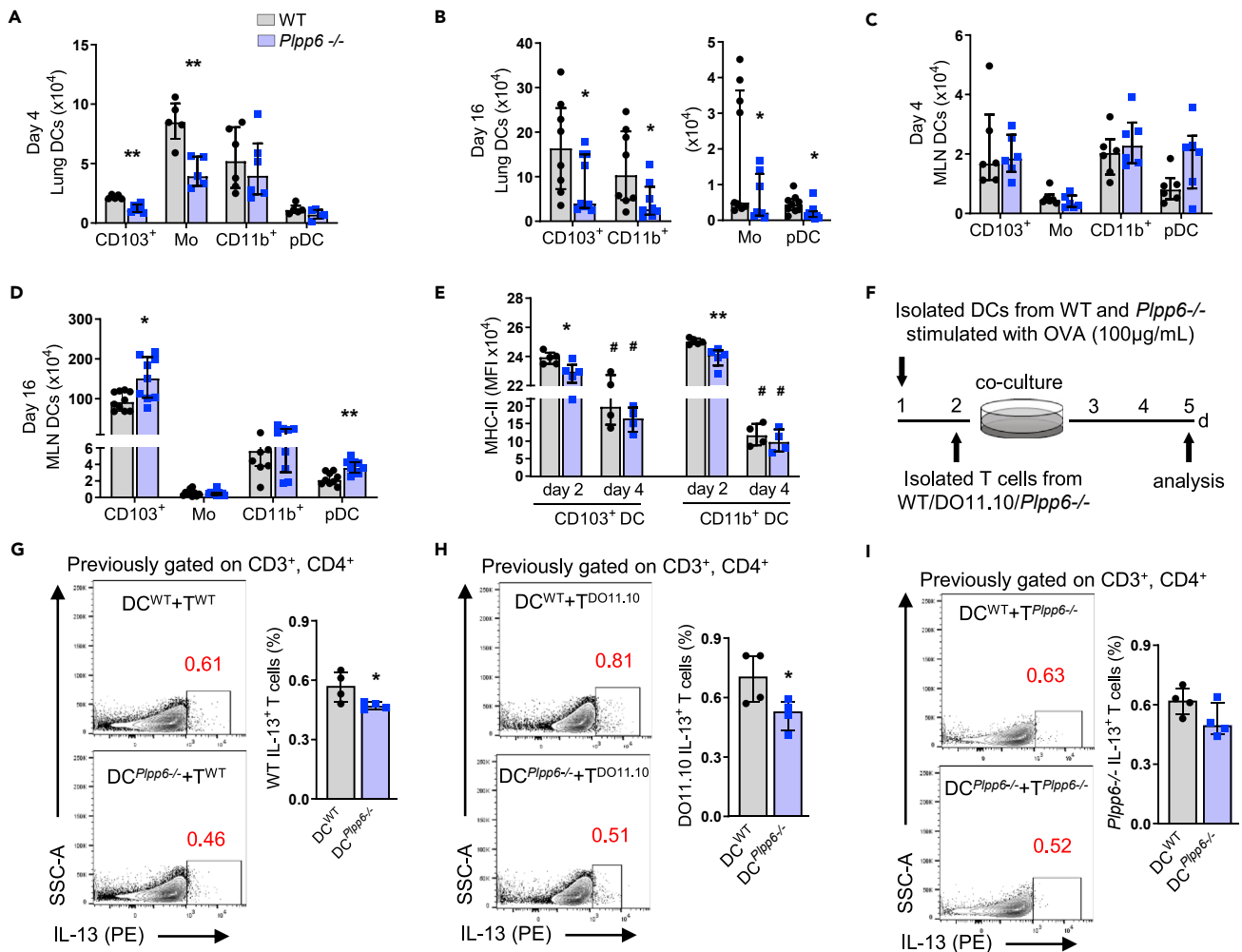


Figure 4. *Ppp6*^{-/-} mice have decreased allergen-induced lung DC numbers and function

Numbers and activation of lung and MLN DCs were determined on day 2, day 4, and day 16 of the HDM protocol. (A and B) Lung DC subsets (CD103⁺ DC, monocyte-derived DC (Mo), CD11b⁺ DC, and pDC) numbers on day 4 and day 16 of the HDM protocol, respectively; experiments were performed 3 times for a total of n = 5 to 10. (C and D) MLNs DC subsets on day 4 and day 16 of the HDM protocol, respectively; experiments were performed 3 times for a total of n = 5 to 10. (E) Mean fluorescent intensity (MFI) of MHC-II expression on CD103⁺ DCs and CD11b⁺ DCs from MLNs on day 2 and day 4 of HDM protocol; experiments were performed 2 times for a total of n = 4 to 5. (F) Illustration of DC-T cell co-culture model (see STAR Methods). (G–I) Percentage of WT IL-13⁺ CD4⁺ T cells, DO11.10 IL-13⁺ CD4⁺ T cells and *Ppp6*^{-/-} IL-13⁺ CD4⁺ T cells, respectively, co-cultured with DCs from WT or *Ppp6*^{-/-} mice (representative flow cytometry plots on the left; numbers in red represent percentages of IL-13⁺ T cells); experiments were performed 2 times for a total of n = 4. *p < 0.05, **p < 0.01 comparing WT and *Ppp6*^{-/-} and #p < 0.05 comparing day 4 and day 2 within same mouse genotype by unpaired nonparametric Mann-Whitney test. Bars represent median with interquartile range. See also Figure S6.

lung, the MLN DC HDM-AF647⁺ MFI was decreased in *Ppp6*^{-/-} mice, especially in CD103⁺ DCs and CD11b⁺ DCs (Figures S6I–S6L).

To determine if the decreased DC antigen uptake in the *Ppp6*^{-/-} mice was related to the decreased allergic lung inflammation in these mice, we next exposed WT and *Ppp6*^{-/-} BMDCs *in vitro* to HDM and adoptively transferred the cells into non-sensitized WT recipient animals (Figure 6A). One week after adoptive transfer, the recipient mice were airway challenged with HDM for 3 days (protocol days 7, 8, and 9) and immunophenotyped 24h after the last HDM challenge on protocol day 10 (Figure 6A). The recipient WT mice that were given *Ppp6*^{-/-} BMDCs had significantly lower numbers of lung Eos, T cells, and aMacs relative to mice that received WT BMDCs by adoptive transfer (Figure 6B). Significantly lower numbers of lung DCs but not

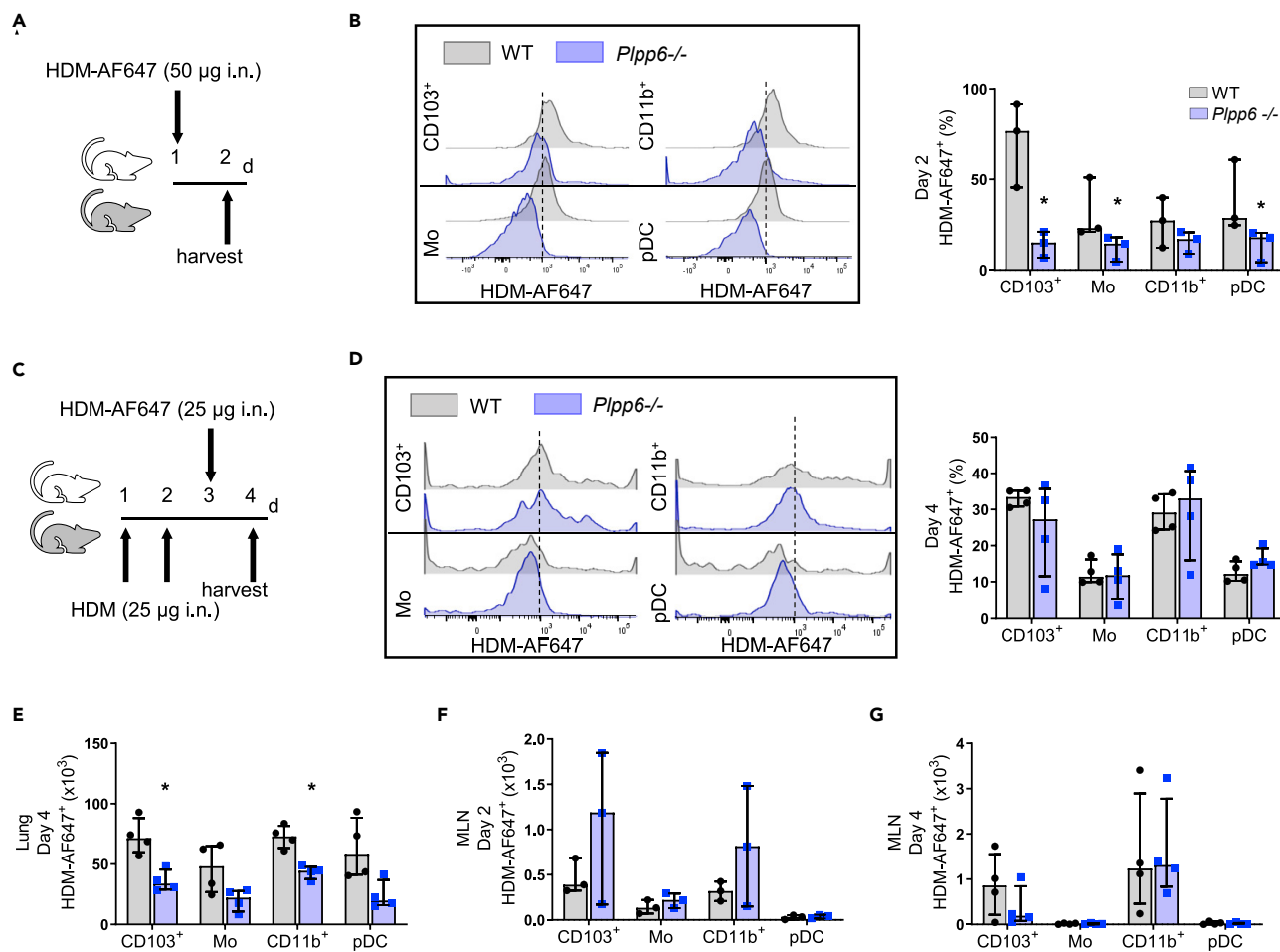


Figure 5. *Plpp6*^{-/-} mice have decreased *in vivo* DC allergen uptake and allergic lung inflammation

(A and B) Mice received one dose of labeled HDM (HDM-AF647) and the percentage of lung HDM-AF647⁺ DC subsets was determined by FACS (representative flow cytometry histograms top panel) 1 day after HDM-AF647 instillation; experiments were performed 2 times for a total of n = 3. (C and D) Mice received 2 doses of unlabeled HDM on days 1 and 2 followed by one dose of HDM-AF647 on day 3 and the percentages of lung HDM-AF647⁺ DC subtypes were determined by FACS (representative flow cytometry histograms top panel) on day 4; experiments were performed 2 times for a total of n = 4.

(E) MFI of HDM-AF647⁺ DC subsets in the lung on day 4 (n = 4).

(F and G) MFI of HDM-AF647⁺ DC subsets in the MLN on days 2 and 4, respectively (n = 3 to 4). *p < 0.05 comparing WT and *Plpp6*^{-/-} by unpaired nonparametric Mann-Whitney test. Bars represent median with interquartile range. See also Figure S6.

MLN DCs were also present at protocol day 10 after adoptive transfer with *Plpp6*^{-/-} BMDCs (Figures 6C and 6D). Together, these data indicate that PLPP6 contributes to DC allergen uptake and that protection from allergic lung inflammation was in part transferrable by the introduction of *Plpp6* deficient DCs into the airway.

DISCUSSION

Here we provide evidence that murine PLPP6 is a polyisoprenyl diphosphate phosphatase that participates in isoprenoid and cholesterol metabolism as well as immune responses to environmental stimuli. DC cholesterol and macropinocytosis were decreased in *Plpp6*^{-/-} mice, impacting DC antigen uptake and subsequent induction of adaptive immune responses for allergic lung inflammation. Together, these findings support a previously unappreciated role for PLPP6 in DC function and host inflammatory responses to allergen.

The murine PLPP6 homolog displayed substrate preferences that were similar to human PLPP6 (Fukunaga et al., 2006). At the amino acid level, PLPP6 shares structural homology with members of a family of integral

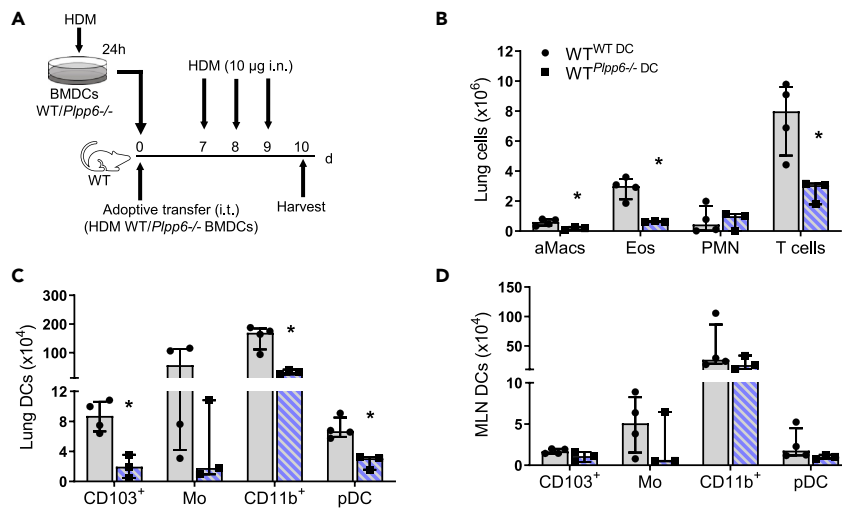


Figure 6. Sensitization with *Plpp6*^{-/-} DCs led to decreased *in vivo* allergic lung inflammation

(A) Adoptive transfer protocol (see STAR Methods); briefly, WT and *Plpp6*^{-/-} BMDCs were generated and exposed *in vitro* to HDM for 24h and then equal DC numbers were adoptively transferred (i.t., 10⁶) into WT mice (day 0). On protocol days 7, 8, and 9, mice were challenged with HDM (i.n., 10 μg), and leukocyte differential cell counts in lung and MLN were determined on day 10.

(B) Lung leukocyte differential cell numbers of aMacs, Eos, PMN, and T cells were determined by FACS; experiments were performed 2 times for a total of n = 3 to 4.

(C and D) Lung and MLNs DC subsets (CD103⁺, Mo, CD11b⁺ and pDC) numbers, respectively, were determined by FACS; experiments were performed 2 times for a total of n = 3 to 4. *p < 0.05 comparing WT and *Plpp6*^{-/-} by unpaired nonparametric Mann-Whitney test. Bars represent median with interquartile range.

membrane lipid phosphate phosphatases/phospho-transferases, including domains critical for enzymatic activity; however, PLPP6 appears to be unique in this larger family for its efficient use of polyisoprenyl phosphates as substrates (Carlo et al., 2009; Fukunaga et al., 2006; Miriyala et al., 2010). Here, we show that the murine homolog for PLPP6 had similar catalytic activity as human PLPP6 (Carlo et al., 2009). In addition to PSDP, PLPP6 can dephosphorylate FDP and select additional phosphorylated lipids *in vitro*, and its over-expression can negatively affect cell growth, morphology, and viability (Miriyala et al., 2010). *Plpp6* expression in leukocytes and how it changes with cell activation point to a role in inflammatory responses. PLPP6 expression decreases in human asthma (Gordon et al., 2016; <https://asthma.cellgeni.sanger.ac.uk/>, Access date: December 10 2021), and here murine *Plpp6* expression decreased in the lungs following allergic inflammation, suggesting similar regulatory mechanisms in human and mice. To investigate the impact of decreased *Plpp6* expression *in vivo* in lung and leukocyte responses, *Plpp6*^{-/-} mice were generated.

Plpp6^{-/-} mice displayed marked differences from WT when challenged with environmental stimuli. Inhaled allergens are detected by airway DCs that can evoke inflammatory responses (Plantinga et al., 2013). DCs are professional antigen-presenting cells that capture, and in some cases present, allergen to naive T cells to initiate their maturation into polarized effector lymphocytes as a part of an adaptive immune response (Fahy, 2015). Here, in a model of allergen sensitization and challenge with the common clinical allergen HDM, DCs and effector T cells along with their proinflammatory products were relatively lower in *Plpp6*^{-/-} mice, suggesting that DC PLPP6 activity facilitates early allergen-initiated immune responses.

Because DCs serve a pivotal role in the initiation of inflammatory responses that when excessive are linked to immunopathology, we next examined lung DCs in more detail. At baseline, lung CD103⁺ DCs and CD11b⁺ DCs express *Plpp6* (Heng et al., 2008), suggesting functional roles for PLPP6 in these DC subsets. With HDM challenge, *Plpp6*^{-/-} mice had significantly fewer numbers of all the induced lung DCs evaluated here, namely CD103⁺ DCs, MoDCs, CD11b⁺ DCs, and pDCs. In contrast to lung DC subsets, *Plpp6*^{-/-} mice had increased numbers of CD103⁺ DCs and pDCs in MLNs after the allergen challenge, supporting distinct mechanisms for DC accumulation and egress in the lung and MLNs. CD103⁺ DCs and pDCs have been assigned regulatory roles for inflammation, including for Th2 and Th17 *in vivo* responses to the HDM

challenge (Conejero et al., 2017; de Heer et al., 2004; Lewkowich et al., 2008). Mice lacking CD103⁺ DCs or pDCs develop exacerbated allergic airway inflammation (Conejero et al., 2017; de Heer et al., 2004), so an increase in lung draining MLN CD103⁺ DCs and pDCs after allergen challenge suggests a regulatory mechanism for those cells in *Plpp6*^{-/-} mice.

Endocytosis of potential airway stimuli by DCs is a major function of these cells in sampling the mucosal environment and directing immune responses (Plantinga et al., 2013). *Plpp6*^{-/-} CD103⁺ DCs and CD11b⁺ DCs had decreased antigen uptake of HDM-AF647, a process that largely proceeds via macropinocytosis (Sallusto et al., 1995). DC macropinocytosis may also be impacted by cell cholesterol content. Cholesterol-depleted BMDCs have defective macropinosome formation and are unable to internalize dextran via macropinocytosis (Sallusto et al., 1995). The *Plpp6*^{-/-} DCs had lower cellular cholesterol content, and cholesterol loading of the *Plpp6*^{-/-} DCs corrected the macropinocytosis defect. Cholesterol is an integral constituent of cell membranes and contributes to cellular homeostasis, particularly as an essential component of lipid rafts for vesicular trafficking and signal transduction (Maxfield and Tabas, 2005). For DC function, cholesterol depletion of antigen-loaded DCs reduces MHC-II expression and affects their capacity to activate T cells (Fessler, 2015). In addition to macropinocytosis, the uptake of HDM can also occur via toll-like receptor 4, which is anchored by lipid rafts (Ryu et al., 2013). Although the nature and content of lipid rafts were not directly evaluated here, they were likely disrupted in the *Plpp6* deficient cells as *Plpp6* expression regulated DC cholesterol content and macropinocytosis, and the altered cellular endocytosis was reversed with cholesterol loading.

Plpp6 deficiency increased PIPP levels by decreasing isoprenyl diphosphate conversion to their corresponding isoprenyl monophosphate during inflammatory responses to HDM. Of interest, *Plpp6*^{-/-} mice still had detectable PSMP at baseline, suggesting the presence of additional or compensatory metabolic pathways for PSMP. PSMP has approximately 2-log orders less bioactivity than PSDP (Bonnans et al., 2006; Levy et al., 1999), so the impact of this residual PSMP on the phenotype of the *Plpp6*^{-/-} mice is not expected to be substantial. The baseline reduction in serum total cholesterol and BMDC cholesterol levels in the *Plpp6*^{-/-} mice are in alignment with earlier observations that increased levels of isoprenyl diphosphates can provide negative feedback to inhibit upstream cholesterol biosynthetic enzymes (Brown and Goldstein, 1980). Depletion of PLPP6 and inhibition of isoprenyl diphosphate catabolism is likely to have a significant impact on gene expression and cell metabolism; topics that will be the subject of future investigation. Of note, the disruption of cholesterol biosynthesis with HMG-CoA reductase inhibition by statins decreases both non-sterol isoprenoids as well as cholesterol, while squalene synthase inhibition with squalenyl 1 lowers cholesterol but not the non-sterol isoprenoids. When hepatocytes are exposed to either a statin or squalenyl 1, there are substantial differences in gene expression that are likely explained in part by differences in isoprenyl diphosphate catabolism (Rondini et al., 2016). Here, *Plpp6* deficiency prevented isoprenyl diphosphate catabolism, suggesting protective roles for the isoprenyl diphosphates and lower cholesterol. Some shorter chain isoprenyl diphosphates may serve as phospho-antigens and augment lung immune response to allergen (Bratt et al., 2018), but targeting *Plpp6* led to less lung allergic inflammation, suggesting a broader regulatory effect for phagocyte function that in aggregate was protective. These findings identify PLPP6 as a new regulatory checkpoint for cholesterol biosynthesis and allergic inflammation. The published impact of statins on endocytosis and inflammatory responses is inconsistent and context-dependent, but in aggregate is also suggestive of a protective action (Parihar et al., 2019).

Endocytosis by professional phagocytes is essential for initiating and regulating inflammatory responses to diverse environmental stimuli. Macropinocytosis is a specialized form of endocytosis that enables lung DCs to serve as pivotal sentinels for inhaled challenges. DC initiation of adaptive inflammatory responses is host protective except in excess when it can lead to immunopathology, as in asthma. Here, we have identified murine PLPP6 as a polyisoprenyl diphosphate phosphatase that is activated in DCs after airway exposure to the common household aeroallergen HDM. *Plpp6* deficiency impacted isoprenoid and cholesterol tone in DCs to decrease allergen uptake by macropinocytosis and restrain allergic lung inflammation. These data have uncovered a role for PLPP6 in macropinocytosis that could serve as a pharmacological target to modulate cholesterol biosynthesis and excess inflammatory responses to allergens.

Limitations of the study

The study has some inherent limitations related to the global knockout of *Plpp6*. In addition to DCs, there may have been other cell types that contributed to the observed *in vivo* phenotype. In addition, the

metabolic changes in cholesterol content were apparent in inbred laboratory mice but may be subject to dietary regulation in WT animals or humans.

DATA AND MATERIALS AVAILABILITY

The data supporting the results in this study are available within the article and in its [supplemental information](#).

STAR★METHODS

Detailed methods are provided in the online version of this paper and include the following:

- KEY RESOURCES TABLE
- RESOURCE AVAILABILITY
 - Lead contact
 - Materials availability
 - Data and code availability
- EXPERIMENTAL MODEL AND SUBJECT DETAILS
- METHOD DETAILS
 - Induction of allergic airway responses
 - Airway responsiveness measurement
 - Real-time quantitative polymerase chain reaction (RT-qPCR)
 - *In vitro* phosphatase assay
 - Thin-layer chromatography (TLC)
 - Liquid chromatography-tandem mass spectrometry (LC-MS/MS)
 - Histology
 - Flow cytometry
 - Cytokine levels
 - IgE quantification
 - Dendritic cell and T cell (DC-T cell) co-culture
 - *In vivo* DC antigen uptake
 - Bone marrow dendritic cells (BMDCs) generation
 - Adoptive transfer of BMDCs
 - Cholesterol measurement
 - Cholesteryl-ester uptake
 - Evaluation of macropinocytosis
- QUANTIFICATION AND STATISTICAL ANALYSIS

SUPPLEMENTAL INFORMATION

Supplemental information can be found online at <https://doi.org/10.1016/j.isci.2022.105185>.

ACKNOWLEDGMENTS

We would like to thank Guangli Zhu for the technical support.

Funding: This work was supported in part by funds from the National Institutes of Health, United States R01HL122531, P01GM0955467 (B.D.L.) and from the United States Department of Defense W81XWH-19-1-0626 (S.F.O.).

AUTHOR CONTRIBUTIONS

T.R.B., T.C., N.K., M.G.D., R.-E.E.A., P.H.Y., H.F., R.H.C., B.G., and S.F.O. designed and performed the experiments, analyzed the data, and performed the statistical analysis. T.R.B and J.N wrote the article. B.D.L. conceived the study, designed the experiments, analyzed the data, and wrote the article.

DECLARATION OF INTERESTS

B.D.L. reports consulting for AstraZeneca, Gossamer Bio, and Pieris Pharmaceuticals on clinical asthma. The other authors declare that they have no competing financial interests related to the publication of this article.

Received: April 12, 2022

Revised: May 11, 2022

Accepted: September 19, 2022

Published: October 21, 2022

REFERENCES

- Bligh, E.G., and Dyer, W.J. (1959). A rapid method of total lipid extraction and purification. *Can. J. Biochem. Physiol.* **37**, 911–917.
- Bonnans, C., Fukunaga, K., Keledjian, R., Petasis, N.A., and Levy, B.D. (2006). Regulation of phosphatidylinositol 3-kinase by polyisoprenyl phosphates in neutrophil-mediated tissue injury. *J. Exp. Med.* **203**, 857–863.
- Bratt, J.M., Chang, K.Y., Rabowsky, M., Franzi, L.M., Ott, S.P., Filosto, S., Goldkorn, T., Arif, M., Last, J.A., Kenyon, N.J., and Zeki, A.A. (2018). Farnesyltransferase inhibition exacerbates eosinophilic inflammation and airway hyperreactivity in mice with experimental asthma: the complex roles of ras GTPase and farnesylpyrophosphate in type 2 allergic inflammation. *J. Immunol.* **200**, 3840–3856.
- Brown, M.S., and Goldstein, J.L. (1980). Multivalent feedback regulation of HMG CoA reductase, a control mechanism coordinating isoprenoid synthesis and cell growth. *J. Lipid Res.* **21**, 505–517.
- Carlo, T., Petasis, N.A., and Levy, B.D. (2009). Activation of polyisoprenyl diphosphate phosphatase 1 remodels cellular presqualene diphosphate. *Biochemistry* **48**, 2997–3004.
- Commisso, C., Flinn, R.J., and Bar-Sagi, D. (2014). Determining the macropinocytic index of cells through a quantitative image-based assay. *Nat. Protoc.* **9**, 182–192.
- Conejero, L., Khouili, S.C., Martínez-Cano, S., Izquierdo, H.M., Brandi, P., and Sancho, D. (2017). Lung CD103+ dendritic cells restrain allergic airway inflammation through IL-12 production. *JCI Insight* **2**, 90420.
- de Heer, H.J., Hammad, H., Soullié, T., Hijdra, D., Vos, N., Willart, M.A.M., Hoogsteden, H.C., and Lambrecht, B.N. (2004). Essential role of lung plasmacytoid dendritic cells in preventing asthmatic reactions to harmless inhaled antigen. *J. Exp. Med.* **200**, 89–98.
- Fahy, J.V. (2015). Type 2 inflammation in asthma—present in most, absent in many. *Nat. Rev. Immunol.* **15**, 57–65.
- Fanta, C.H. (2009). *Asthma*. *N. Engl. J. Med.* **360**, 1002–1014.
- Fessler, M.B. (2015). Regulation of adaptive immunity in health and disease by cholesterol metabolism. *Curr. Allergy Asthma Rep.* **15**, 48.
- Fukunaga, K., Arita, M., Takahashi, M., Morris, A.J., Pfeffer, M., and Levy, B.D. (2006). Identification and functional characterization of a presqualene diphosphate phosphatase. *J. Biol. Chem.* **281**, 9490–9497.
- Gordon, E.D., Simpson, L.J., Rios, C.L., Ringel, L., Lachowicz-Scroggins, M.E., Peters, M.C., Wesolowska-Andersen, A., Gonzalez, J.R., MacLeod, H.J., Christian, L.S., et al. (2016). Alternative splicing of interleukin-33 and type 2 inflammation in asthma. *Proc. Natl. Acad. Sci. USA* **113**, 8765–8770.
- Grimmer, S., van Deurs, B., and Sandvig, K. (2002). Membrane ruffling and macropinocytosis in A431 cells require cholesterol. *J. Cell Sci.* **115**, 2953–2962.
- Gueders, M.M., Paulissen, G., Crahay, C., Quesada-Calvo, F., Hacha, J., Van Hove, C., Tournoy, K., Louis, R., Foidart, J.M., Noël, A., and Cataldo, D.D. (2009). Mouse models of asthma: a comparison between C57BL/6 and BALB/c strains regarding bronchial responsiveness, inflammation, and cytokine production. *Inflamm. Res.* **58**, 845–854.
- Heng, T.S.P., and Painter, M.W.; Immunological Genome Project Consortium (2008). The Immunological Genome Project: networks of gene expression in immune cells. *Nat. Immunol.* **9**, 1091–1094. <https://asthma.cellgeni.sanger.ac.uk/>.
- Khare, A., Krishnamoorthy, N., Oriss, T.B., Fei, M., Ray, P., and Ray, A. (2013). Cutting edge: inhaled antigen upregulates retinaldehyde dehydrogenase in lung CD103+ but not plasmacytoid dendritic cells to induce Foxp3 de novo in CD4+ T cells and promote airway tolerance. *J. Immunol.* **191**, 25–29.
- Krishnamoorthy, N., Douda, D.N., Brüggemann, T.R., Ricklefs, I., Duvall, M.G., Abdulnur, R.E.E., Martinod, K., Tavares, L., Wang, X., Cernadas, M., et al. (2018). Neutrophil cytoplasts induce TH17 differentiation and skew inflammation toward neutrophilia in severe asthma. *Sci. Immunol.* **3**, ea04747.
- Krishnamoorthy, N., Oriss, T.B., Paglia, M., Fei, M., Yarlagadda, M., Vanhaesebroeck, B., Ray, A., and Ray, P. (2008). Activation of c-Kit in dendritic cells regulates T helper cell differentiation and allergic asthma. *Nat. Med.* **14**, 565–573.
- Levy, B.D., Fokin, V.V., Clark, J.M., Wakelam, M.J., Petasis, N.A., and Serhan, C.N. (1999). Polyisoprenyl phosphate (PIPP) signaling regulates phospholipase D activity: a 'stop' signaling switch for aspirin-triggered lipoxin A4. *FASEB J.* **13**, 903–911.
- Levy, B.D., Petasis, N.A., and Serhan, C.N. (1997). Polyisoprenyl phosphates in intracellular signalling. *Nature* **389**, 985–990.
- Lewkowich, I.P., Lajoie, S., Clark, J.R., Herman, N.S., Sproles, A.A., and Wills-Karp, M. (2008). Allergen uptake, activation, and IL-23 production by pulmonary myeloid DCs drives airway hyperresponsiveness in asthma-susceptible mice. *PLoS One* **3**, e3879.
- Maxfield, F.R., and Tabas, I. (2005). Role of cholesterol and lipid organization in disease. *Nature* **438**, 612–621.
- Miriyala, S., Subramanian, T., Panchatcharam, M., Ren, H., McDermott, M.I., Sunkara, M., Drennan, T., Smyth, S.S., Spielmann, H.P., and Morris, A.J. (2010). Functional characterization of the atypical integral membrane lipid phosphatase PDP1/PPAPDC2 identifies a pathway for interconversion of isoprenols and isoprenoid phosphates in mammalian cells. *J. Biol. Chem.* **285**, 13918–13929.
- Nathan, C. (2002). Points of control in inflammation. *Nature* **420**, 846–852.
- Packard, R.R.S., Maganto-García, E., Gotsman, I., Tabas, I., Libby, P., and Lichtman, A.H. (2008). CD11c(+) dendritic cells maintain antigen processing, presentation capabilities, and CD4(+) T-cell priming efficacy under hypercholesterolemic conditions associated with atherosclerosis. *Circ. Res.* **103**, 965–973.
- Parihar, S.P., Guler, R., and Brombacher, F. (2019). Statins: a viable candidate for host-directed therapy against infectious diseases. *Nat. Rev. Immunol.* **19**, 104–117.
- Plantinga, M., Guilliams, M., Vanheerswyngheles, M., Deswarte, K., Branco-Madeira, F., Toussaint, W., Vanhoutte, L., Neyt, K., Killeen, N., Malissen, B., et al. (2013). Conventional and monocyte-derived CD11b(+) dendritic cells initiate and maintain T helper 2 cell-mediated immunity to house dust mite allergen. *Immunity* **38**, 322–335.
- Rondini, E.A., Duniec-Dmuchowski, Z., Cukovic, D., Dombkowski, A.A., and Kocarek, T.A. (2016). Differential regulation of gene expression by cholesterol biosynthesis inhibitors that reduce (Pravastatin) or enhance (squalstatin 1) nonsterol isoprenoid levels in primary cultured mouse and rat hepatocytes. *J. Pharmacol. Exp. Ther.* **358**, 216–229.
- Ryu, J.H., Yoo, J.Y., Kim, M.J., Hwang, S.G., Ahn, K.C., Ryu, J.C., Choi, M.K., Joo, J.H., Kim, C.H., Lee, S.N., et al. (2013). Distinct TLR-mediated pathways regulate house dust mite-induced allergic disease in the upper and lower airways. *J. Allergy Clin. Immunol.* **131**, 549–561.
- Sallusto, F., Cella, M., Danieli, C., and Lanzavecchia, A. (1995). Dendritic cells use macropinocytosis and the mannose receptor to concentrate macromolecules in the major histocompatibility complex class II compartment: downregulation by cytokines and bacterial products. *J. Exp. Med.* **182**, 389–400.
- Walker, J.A., and McKenzie, A.N.J. (2018). TH2 cell development and function. *Nat. Rev. Immunol.* **18**, 121–133.

STAR★METHODS

KEY RESOURCES TABLE

REAGENT or RESOURCE	SOURCE	IDENTIFIER
Antibodies		
anti-mouse CD45	Biolegend	clone 30-F11; cat#103130; RRID: AB_893339
anti-mouse CD11c	Biolegend	clone N418; cat#117305; RRID: AB_313774
anti-mouse CD11b	Biolegend	clone M1/70; cat#101211; RRID: AB_312794
anti-mouse Ly6G	Biolegend	clone 1A8; cat#127621; RRID: AB_10640452
anti-mouse CD64	Biolegend	clone X54-5/7.1; cat#139320; RRID: AB_2566559
anti-mouse CD68	Biolegend	clone FA-11; cat#137021; RRID: AB_2616811
anti-mouse MHC-II	Biolegend	clone M5/114.15.2; cat#25-5321-80; RRID: AB_10870792
anti-mouse CD45R (B220)	Biolegend	clone RA3-6B2; cat#12-0452-81; RRID: AB_465671
anti-mouse CD103	Biolegend	clones 2E7 and M290; cat#121413 and cat#563087; RRID: AB_1227503 and AB_2721775
anti-mouse CD86	Biolegend	clone GL-1; cat#105011; RRID: AB_493343
anti-mouse CD40	Biolegend	clone 3/23; cat#124609; RRID: AB_1134084
anti-mouse CD3	Biolegend	clone 17A2; cat#100219; RRID: AB_1732068
anti-mouse CD4	Biolegend	clone RM4-5; cat#100537; RRID: AB_893331
anti-mouse CD19	Biolegend	clone 1D3/CD19; cat#152403; RRID: AB_2629812
anti-mouse IgM	Biolegend	clone RMM-1; cat#406515; RRID: AB_10690815
anti-mouse IgD	Biolegend	clone 11-26c.2a; cat#405713; RRID: AB_10645480
anti-mouse CCR7	Biolegend	clone 4B12; cat#120105; RRID: AB_389357
anti-mouse Ki-67	Biolegend	clone 16A8; cat# 652405; RRID: AB_2561929
anti-mouse IL-5	Biolegend	clone TRFK5; cat#504306; RRID: AB_315330
anti-mouse lineage antibodies (CD3, Ly-6G/Ly-6C, CD45R, Ter-119, CD11b)	Biolegend	Clones 17A2; RB6-8C5; RA3-6B2; Ter-119; M1/70; cat#100203, 108406, 103205, 116205, 101205; RRID: AB_312660, AB_313371, AB_312990, AB_313706, AB_312788
anti-mouse CD90.2	Biolegend	clone 53-2.1; cat#140307; RRID: AB_10643585
anti-mouse CD25	Biolegend	clone PC 61.5; clone PC 61.5; cat#102007; RRID: AB_312856
anti-mouse CD44	Biolegend	clone IM7; cat#103005; RRID: AB_312956
anti-mouse CD62L	Biolegend	clone MEL-14; cat#104417; RRID: AB_313102
anti-mouse Siglec-F	Thermo Fisher Scientific	clone E50-2440; cat#; RRID: AB_394341
anti-mouse IL-13	Thermo Fisher Scientific	clone eBio 13A; cat# 12-7133-41; RRID: AB_10852712
anti-mouse F4/80	Thermo Fisher Scientific	clone BM8; cat# 25-4801-82; RRID: AB_469653
anti-mouse PDCA1 (CD317)	BD Biosciences	clone 927; cat# 566431; RRID: AB_2739728
Chemicals, peptides, and recombinant proteins		
Plpp6 (NM_028922) Mouse Tagged ORF Clone	OriGene	Cat#: MG204002
Murine GM-CSF recombinant	Peprotech	Cat# AF-315-03
Sphingosine-1-phosphate	Cayman	Cat# 22498
Farnesyl Diphosphate (FPP)	Echelon Biosciences	Cat# I-0150
Phosphatidic acid	Cayman	Cat# 15080
Lysophosphatidic acid	Avanti	Cat# 857130P
Acetone	Milipore Sigma	Cat# 650501
Chloroform	Milipore Sigma	Cat# 34854

(Continued on next page)

Continued

REAGENT or RESOURCE	SOURCE	IDENTIFIER
Methanol	Milipore Sigma	Cat# 34860
sphingosine-1-phosphate-d7	Avanti	Cat# 860659P
Acetonitrile	Milipore Sigma	Cat# 34851
2-Propanol	Milipore Sigma	Cat# 34863
Formic acid 98%–100%	Milipore Sigma	Cat# 5.33002
Phosphate-buffered saline (PBS)	Gibco	Cat# 14190235
10% buffered formalin	Fisher Scientific	Cat# SF100-4

Critical commercial assays

Mouse IL-5 ELISA	Thermo Fisher Scientific	Cat# EMIL5ALPHA
Mouse IL-13 ELISA	Thermo Fisher Scientific	Cat# KMC2221
Mouse IgE ELISA	Biologend	Cat# 432401
Cholesterol Quantitation Kit	Millipore Sigma	Cat# MAK043

Experimental models: Cell lines

293 [HEK-293]	ATCC	Cat# CRL-1573
---------------	------	---------------

Experimental models: Organisms/strains

BALB/c Mice	Charles River	Strain code 028
C.Cg-Tg(DO11.10)10Dlo/J	The Jackson Laboratory	Strain code 003303

Software and algorithms

AriaMX software	Agilent	
FlowJo v10	FlowJo	
ImageJ		

Other

House dust mite (HDM) (<i>Dermatophagoides pteronyssinus</i> , B70 source material)	Greer Labs	Cat# XPB91D3A2.5
TRIZOL Reagent	Thermo Fisher Scientific	Cat# 15596026
TaqMan Reverse Transcription Reagents	Thermo Fisher Scientific	Cat# N8080234
MegaTran 2.0	OriGene	Cat# TT210002
Pierce™ High Capacity Ni-IMAC	Thermo Fisher Scientific	Cat# A50588
Deoxyribonuclease I from bovine pancreas (DNase)	Millipore Sigma	Cat# DN25
Collagenase A	Millipore Sigma	Cat# 10103586001
FBS (heat-inactivated fetal bovine serum)	Denville Scientific	Cat# C788D86
Foxp3 / Transcription Factor Staining Buffer Set	Thermo Fisher Scientific	Cat# 00-5523-00
RPMI-1640 Medium	Millipore Sigma	Cat# R8758
Penicillin-Streptomycin	Gibco	Cat# 15140
Sodium pyruvate solution	Millipore Sigma	Cat# S8636
2-Mercaptoethanol	Millipore Sigma	Cat# M3148
Tonbo Cell Stimulation Cocktail (500X)	Tonbo	Cat# TNB-4975
Sodium Pentobarbital	Abott Laboratories	
Methacholine chloride	Millipore Sigma	Cat# 62-51-1
Lipopolysaccharides from <i>Escherichia coli</i> O55:B5	Millipore Sigma	Cat# L2880
Alexa Fluor 647 Antibody Labeling Kit	Thermo Fisher Scientific	Cat# A20186
Pierce 16% Formaldehyde, Methanol-free	Thermo Fisher Scientific	Cat# 28906
Cholesterol Detection Filipin III	Cayman	Cat# 10009867
Lipoprotein Depleted Fetal Bovine Serum	kalen Biomedical	Cat# 880100-1

(Continued on next page)

Continued

REAGENT or RESOURCE	SOURCE	IDENTIFIER
CholEsteryl BODIPY	Thermo Fisher Scientific	C3927MP
DMSO	Thermo Fisher Scientific	Cat# 022914.M1
Dextran, Tetramethylrhodamine, 70,000 MW, Lysine Fixable	Thermo Fisher Scientific	Cat# D1818
5-(N-Ethyl-N-isopropyl)amiloride	Millipore Sigma	Cat# A3085
Cholesterol-Water Soluble	Millipore Sigma	Cat# C4951

RESOURCE AVAILABILITY

Lead contact

Further information and requests for resources and reagents should be directed to and will be fulfilled by the lead contact Bruce D. Levy (blevy@bwh.harvard.edu).

Materials availability

The mouse line generated in this study is available directly from the authors. This study did not generate additional unique reagents.

Data and code availability

- Mass Spectrometry, flow cytometry, and microscopy data reported in this paper will be shared by the [lead contact](#) upon request.
- No original code is associated with this manuscript.
- Any additional information required to reanalyze the data reported in this paper is available from the [lead contact](#) upon request.

EXPERIMENTAL MODEL AND SUBJECT DETAILS

The experimental animal model used here was induction of allergic airway responses in mice (see below). To determine the impact of *Plpp6* expression, WT and *Plpp6*^{-/-} mice were used. To generate *Plpp6* knockout mice (*Plpp6*^{-/-}), the entire coding region of *Plpp6* was replaced by a neomycin cassette in a PTL1 embryonic stem cell (129B6 hybrid). Germline chimeras were generated by injection of *Plpp6* null embryonic stem cells into Balb/c blastocysts. Male germline chimeras were bred with females of the same strain to transmit the *Plpp6*-null allele. *Plpp6*^{-/-} mice were backcrossed by selectively breeding individuals containing more of the recipient genome from each generation (Marker-Assisted Accelerated Backcrossing (MAX-BAX®) from Charles River) to have a fully congenic colony in 5 generations. *Plpp6* genotype was confirmed by PCR. We chose to backcross to Balb/c because of our earlier results ([Krishnamoorthy et al., 2018](#)) and results in the published literature on allergic lung inflammation in this strain ([Gueders et al., 2009](#)). The WT allele was identified as a 103-nucleotide band using a primer set consisting of *Plpp6* WT forward: 5'-GGCTATTACTGAACACGGCCATAC-3' and *Plpp6* WT reverse: 5'-GAGTCAGCCAGCTTGATTCTTTACA-3'. The *Plpp6* null allele was identified by a 326-nucleotide band using the primers *Plpp6* forward: 5'-CTCCAAGGTACACAGCTTCCTTGTC-3' and *Plpp6* reverse: 5'-CTAGCTTGCTG-GACGTAAACTCCT-3'. WT Balb/c mice were purchased from Charles River Laboratory. C. Cg-Tg (DO11.10) 10 Dlo/J mice were purchased from The Jackson Laboratory. All animals were housed in isolation cages in viral antibody-free conditions. All mice subjected to the protocol were male aged 6 to 8 weeks old. All animal experiments were carried out in accordance with NIH Guidelines for the Care and Use of Laboratory Animals as well as guidelines prescribed by the Institutional Animal Care and Use Committee (IACUC) at Brigham and Women's Hospital (2016N000357) and Harvard Medical Area (05115) (AAALAC 1729).

METHOD DETAILS

Induction of allergic airway responses

Mice (Balb/c) were anesthetized with isoflurane and sensitized with 25µg of house dust mite (HDM) (*Dermatophagoides pteronyssinus*, B70 source material, Greer labs with endotoxin levels of 880 EU/vial

(QCM023)) intranasally (i.n.) in 25 μ L of saline once daily for three days (days 1–3). HDM challenge with 25 μ g (25 μ L) of HDM (i.n.) was performed once daily for 8 days (days 8–15). Naïve mice (non-sensitized or challenged) were used as control. Mice were then euthanized at indicated time points (day 2 or day 4 of sensitization protocol or at day 16 of antigen challenge phase) by an overdose of isoflurane. Blood, lungs, mediastinal lymph nodes (MLNs) and spleens were harvested for analyses.

Airway responsiveness measurement

Mice were anesthetized with pentobarbital (70 mg/kg, intraperitoneally (i. p.); Abbott Laboratories), tracheostomized and mechanically ventilated with a ventilator for small animals (FlexiVent - SCIREQ). The dose response curve was performed exposing anesthetized mice to PBS then sequentially methacholine (MCh) (Sigma-Aldrich) doses of 1, 3, 10, 30 and 100 mg/mL. Airway resistance (Rrs) was determined as the mean of twelve measurements obtained for each concentration of MCh and is reported as percent increase from baseline (PBS nebulization). No lung homogenates or histology were performed on mice that were subjected to measurement of airway responsiveness.

Real-time quantitative polymerase chain reaction (RT-qPCR)

Lungs were harvested and snap frozen. RNA was extracted from lung homogenates using TRIzol® (Thermo Fisher Scientific), then reverse transcribed to complementary DNA (cDNA) using reverse transcription kit (TaqMan®, Thermo Fisher Scientific). The cDNA was used as a template for the amplification of phospholipid phosphatase 1 (*Plpp1*), *Plpp2*, *Plpp3*, *Plpp4*, *Plpp5*, *Plpp6*, interleukin 4 (*il4*), *il5*, *il13*, 3-hydroxy-3-methylglutaryl-Coenzyme A synthase (*Hmgcs*), 3-hydroxy-3-methylglutaryl-Coenzyme A reductase (*Hmgcr*), mevalonate kinase (*Mvk*), farnesyl diphosphate synthase (*Fdps*), geranylgeranyl diphosphate synthase 1 (*ggps1*), farnesyl diphosphate farnesyl transferase 1 (*Fdft1*) (squalene synthase - SQS) and a control housekeeping gene, 18S ribosomal RNA (*18s* rRNA) (all from Integrated DNA Technologies) (primer sequences in Table S1) by RT-qPCR using Agilent AriaMx RT- qPCR machine. Fold change was calculated as $2^{-\Delta\Delta CT}$ for the difference between the cycle threshold (C_T) value for the gene of interest and the respective C_T value for the housekeeping gene (ΔC_T) to naïve. Statistical significance was tested on ΔC_T values.

In vitro phosphatase assay

The assay was performed as in (Carlo et al., 2009). In brief, an expression construct harboring the coding sequence for recombinant mouse (rm) Plpp6 (MR204002, Origene) with 6xHis-tag was transfected (Megatran) into HEK293 cells. 24h after transfection the recombinant protein was captured using nickel-immobilized metal affinity chromatography. Enzymatic activity assays were performed using the partially purified recombinant mouse protein. No human PLPP6 activity endogenous to the cell line was present in these *in vitro* assays. Recombinant mPlpp6 (2 μ g) was added to mixed micelles of select phosphorylated lipids (presqualene diphosphate (PSDP) (isolated as in (Levy et al., 1997)), sphingosine-1-phosphate (S1P) (Cayman), farnesyl diphosphate (FDP) (Echelon), phosphatidic acid (PA) (Cayman) and lysophosphatidic acid (LPA) (Cayman)) (20 μ M) for 30 min at 37°C with gentle mixing. Free phosphate was determined using malachite green detection.

Thin-layer chromatography (TLC)

Lungs from WT and *Plpp6*^{-/-} were harvested at day 16 of the HDM protocol, homogenized using a manual dounce with 1mL of MeOH on ice, saponified with 1 volume of 10% KOH in MeOH for 30 min at 37°C, and then 1 volume of acetone followed by 2-5 volume CHCl₃:MeOH (2:1, v/v) were added. The samples were kept at -20°C overnight and non-saponifiable lipids were isolated as in (Levy et al., 1997). The isolated lipids and related chromatography standards (farnesyl diphosphate (FDP), sphingosine-1-phosphate (S1P) and lysophosphatidic acid (LPA)) were analyzed by silica TLC. The mobile phase was CHCl₃:MeOH:H₂O (65:25:4, v/v) (45min, room temperature (RT), with curtains). The lipids were visualized by exposure to sublimed iodine (20min, RT) followed by lightly sprayed 10% CuSO₄ in 8% phosphoric acid prior to charring (100°C, 20min, followed by 120°C, 10min). Lipids from samples and standards were identified by the R_f values based on published data (Levy et al., 1997), and quantified by densitometry using ImageJ software.

Liquid chromatography-tandem mass spectrometry (LC-MS/MS)

Because PSDP and PSMP are not commercially available as authentic standards, we isolated these lipids from human neutrophils by preparative TLC, as in (Levy et al., 1997). Mouse lungs were collected at day

16 of the HDM protocol and for comparison from antigen naïve mice. The tissue samples (112.5–214.2mg) were homogenized and then extracted by the Bligh and Dyer method (Bligh and Dyer, 1959). Briefly, 1mL of chloroform and 800 μ L of water were added to lung homogenate immersed in 2mL methanol containing an internal standard (100ng deuterated sphingosine-1-phosphate (d7-S1P, Avanti Polar Lipids)). Then, samples were vortexed briefly and sonicated for 10min. Subsequently, 1mL of chloroform and 1mL of water were added to samples and centrifugation (2000g, 10min) was conducted for phase separation. Lower phase was recovered and brought to dryness under nitrogen. The dried samples were reconstituted in 200 μ L of acetonitrile. Extracted samples were analyzed with a Vanquish UPLC coupled with a Q Exactive Orbitrap (Thermo Scientific). Samples were injected onto a YMC-Triart C8 column (2.1*100mm, 3 μ m). The column flow rate was set to 0.2 mL/min and the column temperature was maintained at 40°C. Four mobile phases were used including water (solvent A), 2-propanol (solvent B), 2% formic acid in water (solvent C), and acetonitrile (solvent D). The elution gradient was employed as follows: 0min, 69% A/1% C/30% D; 1min, 69% A/1% C/30% D; 7min, 4% A/1% C/95% D; 10min, 4% A/1% C/95% D; 10.1min, 4% A/75% B/1% C/20% D; 15min, 4% A/75% B/1% C/20% D; 15.1min, 69% A/1% C/60% D; 20min, 69% A/1% C/60% D. The following MS conditions were used: spray voltage, 3kV; sheath gas, 50AU; auxiliary gas, 15AU; capillary temperature, 320°C; aux gas heater temperature, 30°C; mean collision energy for PRM, 35AU. MS1 spectra were acquired in negative ion mode (R = 70,000 at m/z 200) with an m/z range from 200-700. The parallel reaction monitoring with an inclusion list was performed (R = 17500 at m/z 200) for MS/MS analysis. PSMP was identified by matching their exact masses and retention times based on the biogenic, TLC-purified standards, confirmed with characteristic MS/MS transition (505.3->79.0). The levels of PSMP from each sample were quantified by measuring the peak areas from the extracted ion chromatograms (XICs) from the PRM data. Measured areas were normalized by the area of internal standard and sample weight and normalized relative intensities were averaged in biological replicates and compared between WT and *Plpp6*^{-/-} groups.

Histology

Lungs for histology were perfused with 5mL of phosphate buffered saline (PBS) and fixed with 10% buffered formalin for 24h then kept in 70% ethanol. Paraffin embedded 5 μ m sections of lungs were cut and stained with hematoxylin and eosin (H&E) (Sigma-Aldrich) or periodic acid schiff (PAS) (Sigma-Aldrich). Histology slides pictures were taken with a camera attached to a microscope (Zeiss).

Flow cytometry

Lungs were flushed with 5mL of PBS to clear the red blood cells (RBCs and leukocytes from circulation), then tissue was dissociated using gentleMACS dissociator as per manufacturer's instructions, then incubated for 30 min at 37°C in solution containing DNase (30 μ g/mL) (Sigma-Aldrich) and collagenase A (0.7 mg/mL) (Sigma-Aldrich). MLNs were dissociated using round bottom tube with 40 μ m cell strainer cap using the plunger of 1mL syringe and ice-cold PBS with 2% FBS (heat-inactivated fetal bovine serum) (Denville Scientific). For spleen cells, tissue was dissociated in PBS 2% FBS using gentleMACS dissociator followed by RBC lysis (Thermo Fischer Scientific). Single cell suspensions were fixed and permeabilized to stain for surface and intracellular markers using FoxP3 staining Kit (Thermo Fisher Scientific). For intracellular cytokine assessment, cells were resuspended in complete media (RPMI 1640 with L-glutamine (Sigma-Aldrich) supplemented with 10% FBS, 50U/mL of penicillin and 50 μ g/mL of streptomycin (Gibco), 1mM sodium pyruvate (Sigma-Aldrich) and 50 μ M 2-mercaptoethanol (Gibco)) and then stimulated for 4h with a cell stimulation cocktail (Tonbo biosciences, catalog number TNB-4975) at 37°C. This Tonbo cocktail is composed of the phorbol ester, PMA (Phorbol 12-Myristate 13-Acetate), a calcium ionophore (Ionomycin), and the protein transport inhibitors Brefeldin A and Monensin. This Cell Stimulation Cocktail (500X) is used to elicit cytokine production and retention allowing for detection of intracellular protein by flow cytometry. After stimulation, cells were harvested and stained with live/dead fixable yellow dead cell staining kit (Thermo Fisher Scientific) and then fixed and permeabilized to stain for intracellular cytokines using FoxP3 staining Kit (Thermo Fisher Scientific). The following mouse antibodies were used for cell staining: anti-cluster of differentiation (CD)45 (clone 30-F11), anti-CD11c (clone N418), anti-CD11b (clone M1/70), anti-Ly6G (clone 1A8), anti-CD64 (clone X54-5/7.1), anti-CD68 (clone FA-11), anti-major histocompatibility complex II (MHC-II) (clone M5/114.15.2), anti-CD45R (B220) (clone RA3-6B2), anti-CD103 (clones 2E7 and M290), anti-CD86 (clone GL-1), anti-CD40 (clone 3/23), anti-CD3 (clone 17A2), anti-CD4 (clone RM4-5), anti-CD19 (clone 1D3/CD19), anti-IgM (clone RMM-1), anti-IgD (clone 11-26c.2a), anti-C-C chemokine receptor type 7 (CCR7) (clone 4B12), anti-Ki-67 (clone 16A8), anti-IL-5 (clone TRFK5), anti-lineage antibodies (clones 145-2C11; RB6-8C5; RA3-6B2; Ter-119; M1/70) and anti-CD90.2 (clone 53-2.1) were purchased from Biogegend.

Anti-Siglec-F (clone E50-2440) and anti-IL-13 (clone eBio 13A) were purchased from Thermo Fisher Scientific. Anti-PDCA1 (clone 927) was purchased from BD Biosciences. All flow cytometry data was acquired on BD FACSCanto II and BD FACSFortessa then analyzed using FlowJo v10 software. All leukocytes were considered CD45⁺; alveolar macrophages (aMacs) were CD68⁺, CD11c⁺, CD11b⁻, eosinophils (Eos) were CD68⁻, CD11c⁻, CD11b⁺ and SiglecF⁺, neutrophils (PMN) were CD68⁻, CD11c⁻, CD11b⁺ and Ly6G⁺, T cells were CD3⁺. Dendritic cells were analyzed as in (Khare et al., 2013): CD103⁺ dendritic cells (DCs) (also referred as cDC1) were CD11c⁺, MHC-II^{high}, CD103⁺; monocyte-derived DCs (Mo) were CD11c⁺, MHC-II⁺, CD11b⁺ and CD64⁺; CD11b⁺ DCs (also referred as cDC2) were CD11c⁺, MHC-II⁺, CD11b⁺ and CD64⁻, plasmacytoid DCs (pDCs) were CD11c⁺, CD45R(B220)⁺, MHC-II^{low}, PDCA1⁺, memory B cells were CD3⁻, CD19⁺, CD45R(B220)⁺, IgM⁺, IgD⁻ (see [flow cytometry](#) gating strategy on [Figures S3A, S4A, and S5](#)). Type 2 innate lymphoid cells (ILC2s) were considered lineage negative (Lin⁻), CD45⁺, and Thy1.2⁺ and intracellular type 2 cytokine expression (IL-5⁺ and/or IL-13⁺) was determined by FACS.

Cytokine levels

Lung tissue samples were homogenized for measurement of IL-5 and IL-13 levels using sensitive and specific ELISAs (Thermo Fisher Scientific) per manufacturer's instructions.

IgE quantification

A volume of approximately 400 μ L of blood was collected from inferior vena cava then centrifuged at 3000g for 20min to obtain the serum for total immunoglobulin (Ig)E quantification by enzyme-linked immunosorbent assay (ELISA) (Biolegend) as per manufacturer's instructions.

Dendritic cell and T cell (DC-T cell) co-culture

To increase DC number to sort by FACS, up to 4 WT and 4 *P1pp6*^{-/-} Balb/c mice were exposed to 25 μ g of HDM and 1 μ g of lipopolysaccharide (LPS) in 25 μ L every 24h for 3 days. 24h after the last exposure, mice were euthanized, and lungs and MLNs were processed to obtain single cells suspension as described above. DCs were sorted in a BD FACS Aria as CD45⁺, CD11c⁺, MHC-II⁺ and autofluorescent FITC (macrophages) were excluded. DCs were cultured for 24h in complete media (described above) with 100 μ g/mL of ovalbumin (OVA). For naive T cells sorting, 2 naive WT, 2 *P1pp6*^{-/-} and 2 C. Cg-Tg (DO11.10) 10 Dlo/J mice were euthanized and the spleens were harvested and homogenized, and RBCs lysed. Cell suspensions were stained with the following mouse antibodies: anti-CD3 (clone 17A2), anti-CD4 (clone RM4-5), anti-CD25 (clone PC 61.5), anti-CD44 (clone IM7), anti-CD62L (clone MEL-14). Naive T cells were sorted as CD3⁺, SSCA^{low}, CD4⁺, CD25⁻, CD44^{low} and CD62L^{high}. T cells were cultured with DCs in a 1:10 (DC:Tcell) ratio for 3 days. On day 3 of the co-incubation, cells were stimulated for 4h with cell stimulation cocktail (Tonbo biosciences, catalog number TNB-4975). Cells were harvested and stained in FoxP3 staining Kit (Thermo Fisher Scientific) with the following mouse antibodies with the same clones as described above: anti-CD45, anti-CD3, anti-CD4 and anti-IL-13.

In vivo DC antigen uptake

HDM was conjugated with Alexa Fluor 647 (HDM-AF647) conjugation kit (Thermo Fisher Scientific) as per manufacturer's instruction. Balb/c WT and *P1pp6*^{-/-} mice were sensitized with HDM-AF647. A group of mice received one single shot of HDM-AF647 (50 μ g in 50 μ L) whereas another group received two instillations of regular (non-labeled) HDM (25 μ g in 25 μ L) (day 1 and 2 of the protocol) and the last instillation of HDM-AF647 (25 μ g in 25 μ L) (day 3 of the protocol). Lungs were harvested 24h after the single or last of the three exposures and HDM-AF647⁺ dendritic cells were analyzed by flow cytometry.

Bone marrow dendritic cells (BMDCs) generation

BMDCs were generated as described before (Krishnamoorthy et al., 2008). Balb/c WT and *P1pp6*^{-/-} mice were euthanized then femur and tibia of mice were removed and flushed out the bone marrow using PBS with 2% FBS. Cells were washed and cultured at 1.5 x 10⁶ cells/mL with complete media (described above) supplemented with 10 ng/mL recombinant mouse granulocyte macrophage colony-stimulating factor (rmGM-CSF) (Peprotech). Three days later, cells were fed with fresh medium and cytokine at the same concentration. On day 6, the loosely adherent cells (immature DCs) were harvested and plated in 12-well plates at 10⁶ cell/mL with 10 ng/mL of rmGM-CSF. At this time point, an aliquot of the cells was used to evaluate the number of DCs by flow cytometry. DCs were considered side scatter-(SSCA)^{int}, forward scatter-(FSCA)^{int}, CD11c⁺, MHC-II⁺ and F4/80⁻.

Adoptive transfer of BMDCs

BMDCs from WT and *Plpp6*^{-/-} (Balb/c) mice were generated as described above. On day -1, immature BMDCs were stimulated with HDM (100 µg/mL) for 24h. On day 0, 10⁶ BMDCs were adoptively transferred (i.t.) into WT recipient mice. On day 7, WT mice were challenged with HDM (10µg in 40µL of saline) for 3 consecutive days. On day 10, lungs and MLNs were harvested for analysis.

Cholesterol measurement

Right after euthanasia with isoflurane overdose, serum was obtained as described above then total cholesterol (free cholesterol and cholesteryl-esters) level was determined by cholesterol quantitation kit (Sigma-Aldrich) as per the manufacturer's instructions. To access cellular cholesterol levels, BMDCs were cultured as described above and cholesterol was analysed on day 7. BMDCs were harvested and fixed with paraformaldehyde (PFA) 2% (30min, 4°C) then washed and stained with Filipin III (Cayman) (1h, 4°C) to quantify free cholesterol. After staining, cells were washed and analyzed by flow cytometry.

Cholesteryl-ester uptake

For cholesteryl-ester uptake, BMDCs were cultured for 24h in complete media supplemented with 10% of lipoprotein depleted FBS (LPD-FBS) (Kalen Biomedical). BMDCs (on day 7) were incubated with 1 µg/mL of CholEsteryl-BODIPY (Thermo Fisher Scientific) dissolved in dimethyl sulfoxide (DMSO) for 4h at 37°C. Then cells were fixed using 2% PFA (30min, 4°C), washed and taken to flow cytometry.

Evaluation of macropinocytosis

Macropinocytosis was accessed by exposing BMDCs on day 7 to HDM-AF647 (100 µg/mL) (labeled as described above) or dextran-tetramethylrhodamine (dextran-TMR) (70.000 MW) (Thermo Fisher Scientific) (0.5 mg/mL) for 1h at 37°C. Some cells were incubated with macropinocytosis inhibitor 5-(N-ethyl-N-isopropyl)-Amiloride (EIPA) (Cayman) (25µM) 24h prior to HDM-AF647 or dextran-TMR exposure. After exposure, cells were fixed with 2% PFA (30min, 4°C) and analyzed by flow cytometry and confocal imaging. BMDCs exposed to dextran-TMR were taken to confocal microscope for imaging. Images were acquired in a single z-plane using a Zeiss LSM 800 scanning confocal microscope with a 63 x 1.4 numerical aperture oil immersion objective. Excitation was provided 561 nm laser line for detection of dextran-TMR. Images were collected with Zen 2.3 software (Zeiss) and DIC and fluorescent images were merged for analysis. Images were taken every 14s and combined to make a video of 15s for a total of 105 pictures. For the rescue experiment, *Plpp6*^{-/-} BMDCs (day 7) were exposed to methyl-β-cyclodextrin loaded with cholesterol (mβCD-chol) (Sigma-Aldrich) (160µg of cholesterol per mL) for 1h, 37°C then washed and resuspended in 1mL of complete media. Loaded and unloaded WT and *Plpp6*^{-/-} BMDCs were then exposed to dextran-TMR to assess macropinocytosis by flow cytometry.

QUANTIFICATION AND STATISTICAL ANALYSIS

Statistical differences between two independent groups were determined by either a one-tailed (n = 3 per group) or two-tailed (n > 3 per group) unpaired nonparametric Mann-Whitney test. Results for nonparametric data were expressed as a median with interquartile range and at least 2 independent experiments were performed. Statistical differences between 3 or more groups were determined by one-way ANOVA and Tukey test for multiple comparisons and the results were expressed as mean ± standard error (SE). *P* < 0.05 was defined as statistically significant.